RESEARCH ARTICLE

An investigation of petrochemical emissions during KORUS-AQ: Ozone production, reactive nitrogen evolution, and aerosol production

Young Ro Lee[1], L. Gregory Huey[1],*, David J. Tanner[1], Masayuki Takeuchi[1], Hang Qu[1], Xiaoxi Liu[2], Nga Lee Ng[1], James H. Crawford[3], Alan Fried[4], Dirk Richter[4], Isobel J. Simpson[5], Donald R. Blake[5], Nicola J. Blake[5], Simone Meinardi[5], Saewung Kim[5], Glenn S. Diskin[3], Joshua P. Digangi[3], Yonghoon Choi[3], Sally E. Pusede[6], Paul O. Wennberg[7], Michelle J. Kim[7], John D. Crounse[7], Alex P. Teng[7], Ronald C. Cohen[8], Paul S. Romer[8], William Brune[9], Armin Wisthaler[10,11], Tomas Mikoviny[10], Jose L. Jimenez[4], Pedro Campuzano-Jost[4], Benjamin A. Nault[4,12], Andrew Weinheimer[13], Samuel R. Hall[13], and Kirk Ullmann[13]

Emissions and secondary photochemical products from the Daesan petrochemical complex (DPCC), on the west coast of South Korea, were measured from the NASA DC-8 research aircraft during the Korea-United States Air Quality campaign in 2016. The chemical evolution of petrochemical emissions was examined utilizing near-source and downwind plume transects. Small alkenes, such as ethene (C_2H_4), propene (C_3H_6), and 1,3-butadiene (C_4H_6), dominated the hydroxyl (OH) radical reactivity near the source region. The oxidation of these alkenes in the petrochemical plumes led to efficient conversion of nitrogen oxides (NO_x) to nitric acid (HNO_3), peroxycarboxylic nitric anhydrides (PANs), and alkyl nitrates (ANs), where the sum of the speciated reactive nitrogen contributes more than 80% of NO_y within a few hours. Large enhancements of short-lived NO_x oxidation products, such as hydroxy nitrates (HNs) and peroxyacrylic nitric anhydride, were observed, in conjunction with high ozone levels of up to 250 ppb, which are attributed to oxidation of alkenes such as 1,3-butadiene. Instantaneous ozone production rates, $P(O_3)$, near and downwind of the DPCC ranged from 9 to 24 ppb h^{-1}, which were higher than those over Seoul. Ozone production efficiencies ranged from 6 to 10 downwind of the DPCC and were lower than 10 over Seoul. The contributions of alkenes to the instantaneous secondary organic aerosol (SOA) production rate, P(SOA), were estimated to be comparable to those of more common SOA precursors such as aromatics at intermediate distances from the DPCC. A model case study constrained to an extensive set of observations provided a diagnostic of petrochemical plume chemistry. The simulated plume chemistry reproduced the observed evolution of ozone and short-lived reactive nitrogen compounds, such as PANs and HNs as well as the rate and efficiency of ozone production. The simulated peroxy nitrates (PNs) budget included large contributions (approximately 30%) from unmeasured PNs including peroxyhydroxyacetic nitric anhydride and peroxybenzoic nitric anhydride. The large, predicted levels of these PAN compounds suggest their potential importance in chemical evolution of petrochemical plumes. One unique feature of the DPCC plumes is the substantial contribution of 1,3-butadiene to ozone and potentially SOA production. This work suggests that reductions in small alkene, especially 1,3-butadiene, emissions from the DPCC should be a priority for reducing downwind ozone.

Keywords: PAN, Ozone, Aerosol, Alkenes, Petrochemical

[1] Georgia Institute of Technology, Atlanta, GA, USA

[2] California Air Resources Board, Sacramento, CA, USA

[3] NASA Langley Research Center, Hampton, VA, USA

[4] University of Colorado, Boulder, CO, USA

[5] University of California, Irvine, CA, USA

[6] University of Virginia, Charlottesville, VA, USA

[7] California Institute of Technology, Pasadena, CA, USA

[8] University of California, Berkeley, CA, USA

[9] Pennsylvania State University, State College, PA, USA

[10] University of Oslo, Oslo, Norway

[11] University of Innsbruck, Innsbruck, Austria

[12] CACC, Aerodyne Research, Inc., Billerica, MA, USA

[13] National Center for Atmospheric Research, Boulder, CO, USA

* Corresponding author:
Email: greg.huey@eas.gatech.edu

1. Introduction

Petrochemical facilities emit a variety of volatile organic compounds (VOCs), such as alkenes (e.g., ethene and propene) and aromatics. Many of these VOCs are highly reactive with atmospheric oxidants and are emitted in close proximity to nitrogen oxides (NO_x). Consequently, chemical and physical evolution of petrochemical emissions can lead to ozone and aerosol formation and impact local and regional air quality (Ryerson et al., 2003; Jobson et al., 2004; Gilman et al., 2009). Acute and chronic exposure to primary emissions and secondary products are of large concern due to potential health effects, such as cardiorespiratory problems, and carcinogenic and genotoxic risks (Lippmann, 1991; Snyder, 2002; Cheng et al., 2007; Kirman et al., 2010).

There has been significant research on the effects of petrochemical emissions on air quality. For example, extensive field measurements in the Houston area during the Texas Air Quality Study (TexAQS) 2000 and 2006 campaigns showed that reactive alkenes, such as ethene (C_2H_4) and propene (C_3H_6), in petrochemical plumes were associated with severe O_3 exceedances in the Houston metropolitan area (Ryerson et al., 2003; Gilman et al., 2009; Washenfelder et al., 2010). Fast production of ozone and conversion of NO_x to nitric acid (HNO_3) and peroxycarboxylic nitric anhydrides (PANs) were observed within petrochemical plumes (Ryerson et al., 2003; Neuman et al., 2012). Notably, the formation of short-lived photochemical products, such as hydroxy nitrates (HNs) and peroxyacrylic nitric anhydride (APAN), demonstrated the photo-oxidation of unique petrochemical VOCs emissions with NO_x leading to reactive nitrogen chemistry significantly different than that of typical urban plumes (Roberts et al., 2001; Rosen et al., 2004; Teng et al., 2015). The investigation of primary petrochemical emissions and their downwind evolution formed the basis for mitigation strategies leading to a significant reduction in ozone levels in the greater Houston area (Kim et al., 2011; Johansson et al., 2014; Zhou et al., 2014). In addition, elevated levels of organic aerosol (OA) have been found in industrial plumes that emanated from the Houston Ship Channel (HSC) and are attributed to both higher primary emissions and VOC oxidation rates (Brock et al., 2003; Bahreini et al., 2009).

Over the past decade, there has been a rapid growth of the petrochemical industry in the Asia-Pacific region. South Korea is a major producer of ethene with a production capacity of 9.8 million tons/year in 2019 (Korea Petrochemical Industry Association, 2019). Petrochemical production is driven by both exports and a large domestic demand for plastic resin (International Energy Agency, 2018). Major petrochemical facilities in South Korea are largely located in coastal areas near urban centers. The Daesan petrochemical complex (DPCC), considered here, is located on the west coast of South Korea approximately 80 km southwest of the Seoul Metropolitan Area (SMA). The SMA is home to approximately 50% of the South Korean population. The operations at the DPCC have been growing rapidly since 2005. This is evidenced by one of the largest increases in global NO_2 column densities over the DPCC region from 2005 to 2016 in contrast to the large reduction in NO_2 over SMA during the same period (Duncan et al., 2016). Despite a continual effort in emission reductions, South Korea has experienced severe air pollution problems, where mitigation is a challenge in part due to uncertainties in complex source characteristics and photochemical interaction between local emissions and pollution transport (Kim et al., 2016; Kim et al., 2018; Kim and Lee, 2018; Nault et al., 2018; Jordan et al., 2020; Simpson et al., 2020; Travis et al., 2022).

The Korea-United States Air Quality (KORUS-AQ) field campaign was conducted over the Korean peninsula and surrounding waters from May to June 2016. The heavily instrumented NASA DC-8 research aircraft measured a wide variety of chemical and physical parameters (Crawford et al., 2021). Several studies from KORUS-AQ focused on the impacts of urban emissions such as reactive aromatics and their subsequent photochemistry contributing to ozone and particulate pollution in the SMA (Nault et al., 2018; Peterson et al., 2019; Schroeder et al., 2020; Simpson et al., 2020; Nault et al., 2021). Another important objective of KORUS-AQ was to provide measurements of large industrial emission sources along the west coast of South Korea. Recently, Simpson et al. (2020) provided the VOC source signatures of the DPCC and also characterized the composition of VOCs and their reactivity toward hydroxyl (OH) radical over Seoul. A companion paper by Fried et al. (2020) provided emissions flux estimates of the DPCC and pointed out that the top-down emission estimate for formaldehyde and its precursors is a factor of 4.3 higher than the values in the bottom-up emission inventory.

This work builds upon previous analyses (Fried et al., 2020; Simpson et al., 2020) of DPCC emissions and investigates the plume chemistry leading to ozone production and reactive nitrogen processing. We report airborne observations of primary petrochemical emissions and secondary photochemical products during the KORUS-AQ campaign. Of a total of 20 Research Flights (RFs) by the NASA DC-8 research aircraft, we focus on RFs (i.e., RF11 and RF18 on May 22 and June 5, 2016, respectively) that sampled both fresh and aged petrochemical plumes from the DPCC. We investigate the oxidation of petrochemical VOCs using the observed OH reactivity and the production of reactive nitrogen in evolving DPCC plumes. For the observed downwind plume transects, we estimate the instantaneous O_3 production (PO_3) and efficiency (OPE). The potential for secondary organic aerosol production, P(SOA), is estimated for speciated VOCs. In addition, we utilize a model case study with extensive initial observational constraints to examine the evolution of an example petrochemical plume. Finally, we compare the results to Houston air quality studies and discuss implications for air quality control strategies in South Korea.

2. Methods

2.1. Aircraft instrumentation

A wide range of chemical, physical, and optical measurements were conducted from the NASA DC-8 research
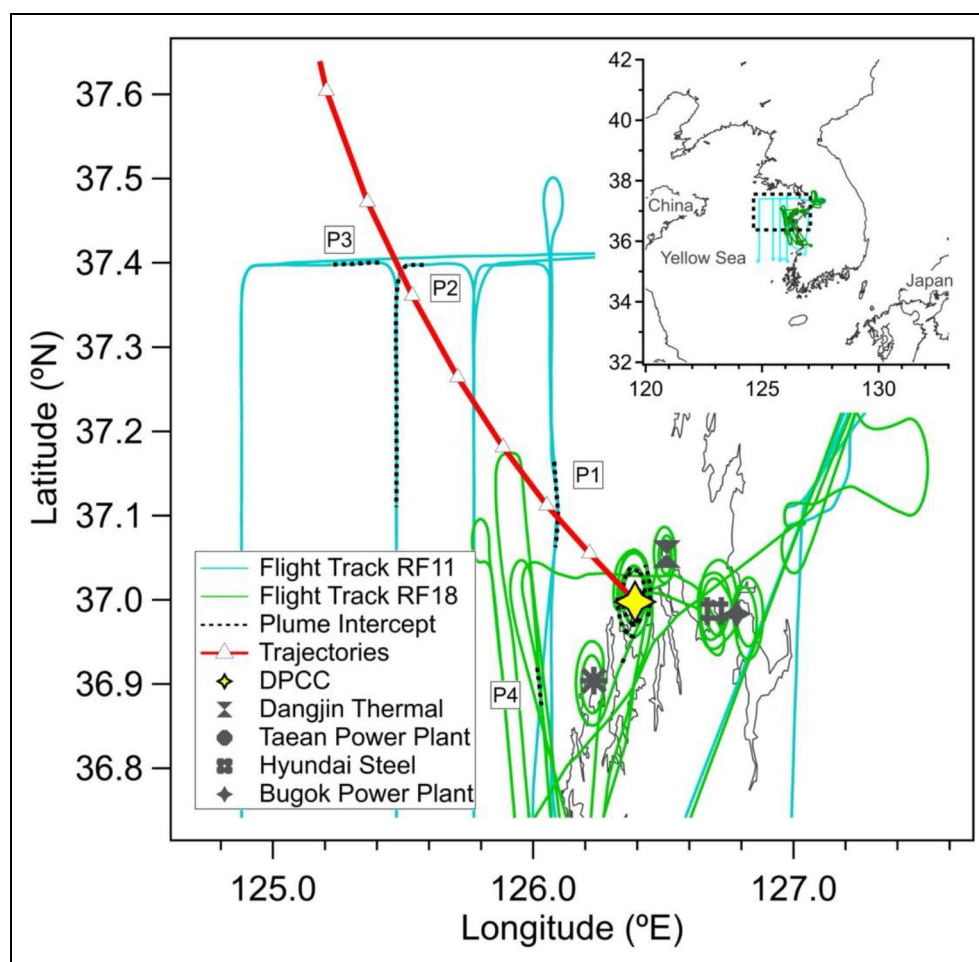
Figure 1. Flight paths of the DC-8 research aircraft and the locations of the Daesan petrochemical complex plume transects (P1–P4) and major industrial facilities (dark gray markers) during RF11 and RF18. The HYSPLIT forward trajectories are shown as red line with open triangles indicating 1-h intervals. The inset shows all DC-8 flight paths during RF11 and RF18, where the dotted rectangle indicates the Daesan area. HYSPLIT = Hybrid Single Particle Lagrangian Integrated Trajectory.

aircraft during the KORUS-AQ campaign. Table S1 summarizes the trace gas measurements utilized in this work, along with methodologies, uncertainties, and references. All aircraft data were synchronized to a common time scale with 1-Hz resolution. The DC-8 data can be accessed through the NASA data archive (https://doi.org/10.5067/Suborbital/KORUSAQ/DATA01).

2.2. Aircraft sampling of DPCC plumes

Figure 1 shows flight paths over the DPCC and the Yellow Sea on 22 May (RF11) and June 5, 2016 (RF18), along with locations of DPCC plume transects (P1–P3 from RF11 and P4 from RF18) and major industrial facilities in the Daesan area. These flights were performed when meteorological conditions allowed the DC-8 to sample industrial emissions with minimal influence of pollutant transport from China and the SMA (Peterson et al., 2019; Simpson et al., 2020). In the busy and restricted airspace over the DPCC and the Yellow Sea, the near-source (RF18) and downwind (RF11) petrochemical plumes were sampled by performing multiple spiral maneuvers and successive distance transects at altitudes ranging from approximately 150 to

400 m above the ground. The pattern was repeated at different times of day to capture different meteorological conditions and variations in emissions from the DPCC.

Table S2 summarizes the local time and location of the plume transects used in this study. The DPCC plume samples (P1–P3) obtained during RF11 are mainly used for the analysis of plume evolution. During RF11, prevailing southeasterly winds at an average wind speed of approximately 4 m s^{-1} provided spatially separated and relatively well-resolved plumes at successive distances downwind of the DPCC. The Hybrid Single Particle Lagrangian Integrated Trajectory model was utilized to perform forward trajectory analysis (Stein et al., 2015) and in general compared well with the locations of the observed DPCC transects during RF11. The 7-h forward trajectory results initialized from 500 m above the ground level at the DPCC on May 22 8:00 (Local Time) are shown in **Figure 1**.

3. Data analysis
3.1. Petrochemical plume identification
Enhancements of CO, CO_2, NO_x, SO_2, HCl, and HCHO were examined as industrial emission tracers to identify and
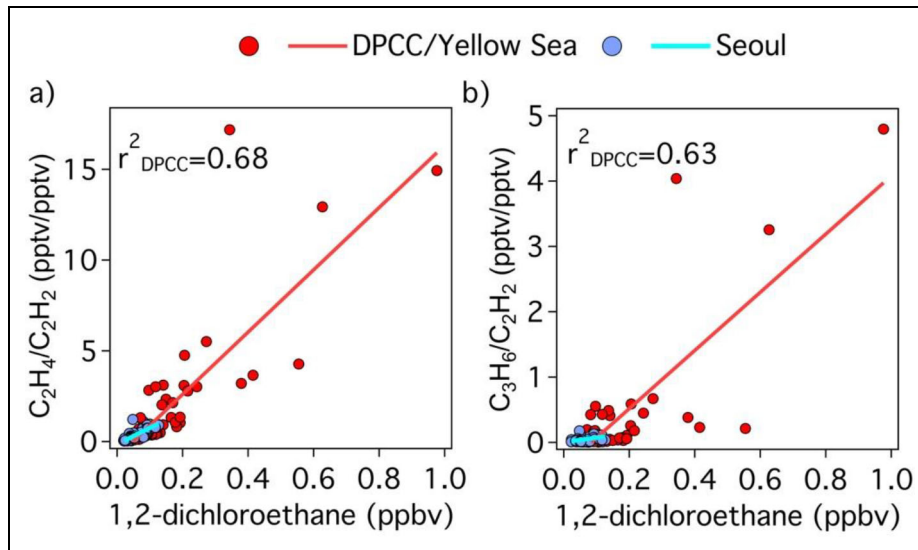
Figure 2. Scatter plots of (a) ethene to ethyne and (b) propene to ethyne ratios versus 1,2-dicholroethane using 1-s data from RF18. Red markers and lines correspond to the measurements over the Daesan petrochemical complex (DPCC) and Yellow Sea and linear regression fit to the data, respectively, where r^2 values for the DPCC/Yellow Sea are included in the upper left. Blue markers and cyan lines correspond to the measurements over Seoul and linear regression fit to the data, respectively. The slopes of the linear regression were 17.2 and 4.5 over the DPCC/Yellow Sea and 9.1 and 0.7 over Seoul for the scatter plots of ethene/ethyne and propene/ethyne versus 1,2-dichloroethane, respectively.

delineate the edges of plume transects (Figure S1). The mixing ratios and relative abundance of VOCs with different chemical reactivity toward OH were used to confirm that enhancements of industrial tracers were due to petrochemical emissions (Simpson et al., 2013). In particular, elevated relative abundances of reactive alkenes, such as ethene and propene (which are relatively short-lived with $\tau_{\mathrm{alkenes}} <1$ day at $[\mathrm{OH}] = 2 \times 10^6$ molecules cm^{-3} and 298 K) to ethyne (C_2H_2), were indicative of petrochemical emissions (Ryerson et al., 2003). In addition, elevated levels of halocarbons were observed in the DPCC plumes (Simpson et al., 2020). **Figure 2** shows the correlation of 1,2-dichloroethane, measured up to 1 ppbv, with the ethene-to-ethyne and propene-to-ethyne ratios. The slopes of the scatter plots and the values of alkenes to ethyne and 1,2-dichloroethane are significantly higher over the DPCC and Yellow Sea than Seoul. For the selected DPCC plume transects, Figure S1 shows the time series of alkenes to ethyne ratios and 1,2-dichloroethane along with the industrial emission tracers.

3.2. Estimation of instantaneous P(O₃) and OPE
The rate of ozone production can be expressed by the sum of reactions of peroxy radicals ($HO_2 + RO_2$) with NO (Equation 1). However, this calculation requires the measurement of peroxy radicals, which are not available in this study.

$$P(O_3) = \Sigma k_{RO_2+NO}[RO_2][NO] + k_{HO_2+NO}[HO_2][NO]. \tag{1}$$

We estimate the instantaneous ozone production rate, P(O₃), and OPE using the method similar to Rosen et al.

(2004) and Perring et al. (2010). The instantaneous P(O₃) is given by:

$$P(O_3) = \Sigma Y_i(1 - \alpha_i)k_{OH+VOC_i}[VOC_i][OH], \tag{2}$$

where Y_i is the number of O₃ molecules produced from the oxidation of VOC$_i$; alkyl nitrate (AN) branching ratios (α_i) represent the probability of peroxy radicals reacting with NO to produce ANs, for which we use literature values (Rosen et al., 2004; Perring et al., 2013; Teng et al., 2015); k_{OH+VOC_i} are the reaction rate coefficients for reaction of VOCs with OH (Atkinson and Arey, 2003); and [OH] and [VOC$_i$] are the concentrations measured by the Airborne Tropospheric Hydrogen Oxides Sensor and Whole Air Sampler (WAS) instruments on board the DC-8 aircraft, respectively. The parameters used in this analysis are summarized in **Table 1**.

We also estimate instantaneous OPE by dividing P(O₃) by the instantaneous production rate of nitric acid (HNO₃) and peroxyacetic nitric anhydride (PAN) calculated using Equations 3–5

$$P_{HNO_3} = k_{OH+NO_2}[OH][NO_2]. \tag{3}$$

$$P_{\text{Peroxy acetyl radical (PA)+PAN}} \cong PAN = \beta_{PAN}k_{OH+\text{acetaldehyde}}[OH][Acetaldehyde], \tag{4}$$

where $\beta_{PAN} = \dfrac{k_{PA+NO_2}[NO_2]}{k_{PA+NO_2}[NO_2]+ k_{PA+NO}[NO] + k_{PA+HO_2}[HO_2]}.$

$$OPE = \frac{P_{O_3}}{P_{HNO_3} + P_{PAN}}. \tag{5}$$

P(O$_3$) and OPE were estimated for P1 and P3, sampled approximately 30 km and 100 km downwind from the DPCC, respectively. Unfortunately, for P2 not enough VOC data was available to estimate P(O$_3$), OPE, and SOA production.

Additionally, an empirical OPE is estimated using the regression of observed odd oxygen, O$_x$ (O$_3$ + NO$_2$), versus the difference between total reactive nitrogen oxides (NO$_y$) and NO$_x$ (e.g., Neuman et al., 2009).

3.3. Estimation of instantaneous SOA production rate

To estimate the effect of photo-oxidation of petrochemical VOCs precursors on SOA production, we calculate the instantaneous SOA production rate, P(SOA), as in Wood et al. (2010). Wood et al. (2010) compared odd oxygen (defined as O$_3$ + NO$_2$) and SOA production rates in Houston and Mexico City. In this work, P(SOA) is estimated using the observed concentrations of VOCs, oxidant, and OA within plume transects and Equation 6 thus differs from net SOA production calculations that require enhancement ratios (e.g., ΔVOCs/ΔCO in the units of µg m^{-3} ppm^{-1}) of VOC precursors and values of OH exposure ([OH]Δt; e.g., Yuan et al., 2013; Nault et al., 2018).

$$P(SOA) = \Sigma \gamma_{SOA_i} k_{OH+VOC_i} [VOC_i][OH]. \quad (6)$$

The categories of VOCs and their associated mass yield at each bin of volatility basis set follow the updated values for high NO$_x$ conditions provided in Ma et al. (2017) and are summarized in Table S3. The OA mass concentrations measured by aerosol mass spectrometer within the selected plume transects are used to calculate an effective SOA yield (γ_{SOA}). Other parameters including the OH rate constant and VOC and OH concentrations are equivalent to the values described in Section 3.2 for calculating P(O$_3$). The SOA yield from ozonolysis is treated identically to that for OH oxidation. VOC oxidation via reaction with the nitrate radical (NO$_3$) during the daytime plume intercepts is assumed to be negligible.

3.4. Model case study of DPCC plumes

Simulation of plume chemistry and comparison to observations requires a complicated treatment of plume chemistry and dispersion, often using a chemical transport model combined with extensive plume sampling to capture emissions, downwind plume structure, and evolution (e.g., Toon et al., 2016). In this work, we did not perform multiple observations of individual plumes as they evolved in time. For this reason, we utilize a model case study to estimate downwind petrochemical plume chemistry using an example plume that allows a general comparison to the downwind DPCC transects in RF11.

In this work, we use a near explicit zero-dimensional model, F0AM (The Framework for 0-D Atmospheric Modeling; Wolfe et al., 2016), with an extensive suite of initial observational constraints to simulate the evolution of an example petrochemical plume over 7 h. This 7-h model integration time was determined based on the downwind distance at P3 from the DPCC (approximately 100 km) and average wind speed (approximately 4 m s^{-1}). After the model was initialized with the observational constraints in Table S4, it was allowed to run freely in time incorporating the Master Chemical Mechanism (MCM) v3.3.1, where meteorological constraints including pressure, temperature, relative humidity, solar zenith angle, and photolysis frequencies (i.e., j-NO$_2$ and j-O$_3$) were taken as the median of the observed values within P1, P2, and P3 in RF11. To account for variability in optical depth, the averaged ratios of the observed and MCM calculated j-NO$_2$ and j-O$_3$ are used to scale all j values by the MCM parameterization (e.g., Wolfe et al., 2014). Background mixing ratios are determined based on the average of measurements made 5s before and after the plume encounter of P1, P2, and P3. The dilution rate coefficient (k_{dil}) is derived from Equation 7, where the Gaussian timescale (τ_{gauss}) is chosen to best-fit the observed downwind CO$_2$ mixing ratios (Alvarado et al., 2015; Wolfe et al., 2022). The initial CO$_2$ mixing ratio is the average of near-source plume measurements during RF18. A dilution lifetime (τ_{dil}) is used for all species in our example plume as an approximation of complex dilution processes in the DPCC plumes, where the averaged τ_{dil} is approximately 6 h derived from the integrated dilution loss rate (i.e., $\Delta t / \int_{t}^{t+\Delta t} k_{dil} dt$). In addition, alkene branching ratios (α) in **Table 1** are used to update the MCM branching ratios (Teng et al., 2015)

$$\frac{dX}{dt} = -k_{dil}\left(X(t) - X_{background}\right), \text{where } k_{dil} = \frac{1}{\tau_{gauss} + 2t}. \quad (7)$$

Initial concentrations of ozone and NO$_x$ are from near-source plume measurements during RF18. As the emissions of VOCs from DPCC show variations on multiple sampling days (Fried et al., 2020), initial concentrations of VOCs, [VOC]$_0$, were estimated from a reverse integration of the first-order loss assumed exclusively from reactions with OH (Equation 8):

$$[VOC]_0 = [VOC]_t e^{k_{OH+VOC_i}[OH]\Delta t}, \quad (8)$$

where [VOC]$_t$ is from the WAS measurement within P1, and $k_{OH + VOC}$ is the reaction rate coefficient. The estimated plume transport (Δt) of 2 h is calculated by dividing downwind distance from the DPCC by average wind speed (approximately 4 m s^{-1}). This results in an approximate OH exposure (i.e., [OH]Δt) of 2 × 10^{10} molecules cm^{-3} s given the transect average OH concentration of 2.7 × 10^6 molecules cm^{-3} at P1. Estimates of OH exposures using alternative methods are discussed in detail in the supporting information (Figure S2). Finally, the calculated initial concentrations of VOCs are compared with the near-source measurements over DPCC from RF18 and summarized along with other model constraints in Table S4.

Table 1. Compound, hydroxy radical reaction rate coefficient (k_{OH}), ozone yield (γ), and alkylnitrate branching ratio (α) for hydrocarbon compounds used in this study

	k_{OH} at 298K	γ[a]	α[b]		k_{OH} at 298K	γ[a]	α[b]
Alkanes							
Ethane	2.48×10^{-13}	2.00	0.019	3-Methylpentane	5.2×10^{-12}	2.85	0.109
Propane	1.09×10^{-12}	2.00	0.036	n-Heptane	6.76×10^{-12}	2.85	0.178
n-Butane	2.36×10^{-12}	2.85	0.077	n-Octane	8.11×10^{-12}	2.85	0.226
i-Butane	2.12×10^{-12}	2.85	0.096	n-Nonane	9.7×10^{-12}	2.85	0.393
n-Pentane	3.8×10^{-12}	2.85	0.105	n-Decane	1.1×10^{-11}	2.85	0.417
i-Pentane	3.6×10^{-12}	2.85	0.07	Cyclopentane	4.97×10^{-12}	2.85	0.045
n-Hexane	5.2×10^{-12}	2.85	0.141	Cyclohexane	6.97×10^{-12}	2.85	0.16
Alkenes				**Aromatics**			
Ethene	8.52×10^{-12}	2	0.013[c]	Benzene	1.22×10^{-12}	2	0.034
Propene	2.63×10^{-11}	2	0.041[c]	Toluene	5.63×10^{-12}	2	0.029
1-Butene	3.14×10^{-11}	2	0.12[c]	Ethylbenzene	7×10^{-12}	2	0.072
cis-2-Butene	5.64×10^{-11}	2	0.12[c]	(m + p)-Xylenes	1.87×10^{-11}	2	0.086
trans-2-Butene	6.4×10^{-11}	2	0.12[c]	o-Xylene	1.36×10^{-11}	2	0.081
1,3-Butadiene	6.66×10^{-11}	2	0.10[c]	Styrene	5.8×10^{-11}	2	0.1
Isoprene	1.0×10^{-10}	2	0.13[c]	1,2,3-Trimethylbenzene	3.27×10^{-11}	2	0.119
α-Pinene	5.23×10^{-11}	2.85	0.18	1,2,4-Trimethylbenzene	3.25×10^{-11}	2	0.105
				1,3,5-Trimethylbenzene	5.67×10^{-11}	2	0.031
Oxygenates				**Others**			
CO	2.39×10^{-13}	1	—	Ethyne	8.74×10^{-13}	1.2	0.09
Formaldehyde	8.37×10^{-12}	1	—	CH$_4$	6.34×10^{-15}	2	—
Formaldehyde (hv)		2	—				
Acetaldehyde	1.58×10^{-11}	3	—				

Reaction rate coefficients with OH (k_{OH}, in units of cm^3 molecule^{-1} s^{-1}) are taken from Atkinson and Arey (2003).

[a]Ozone yields are taken from Rosen et al. (2004).

[b]Alkyl nitrate branching ratios are from Perring et al. (2013) unless noted otherwise.

[c]Hydroxynitrates branching ratios are from Teng et al. (2015).

4. Results and discussion

4.1. Contribution of VOCs to OH reactivity

To investigate the photochemical evolutions of the DPCC emissions, we calculate the contribution of speciated hydrocarbons to the reactivity toward OH (i.e., VOC-OH reactivity) by multiplying the observed concentrations of VOCs from near-source plume samples on June 5, 2016, (RF 18) with the OH reaction coefficients provided in **Table 1** (Equation 9)

$$\text{OH reactivity} = \Sigma k_{OH+VOC_i} \times [VOC_i]. \quad (9)$$

Figure 3a shows the OH reactivity for the near-source transects over the DPCC in the morning during RF 18. The calculated VOC-OH reactivity was up to 33 s^{-1} within the DPCC emissions and was much greater than the values observed over Seoul (up to 7 s^{-1}) during the same flight and from ground-based measurements in the SMA in

spring 2015 (approximately 5 s^{-1}; Kim et al., 2016). The elevated OH reactivity in the DPCC emissions is attributed to anthropogenic alkenes, such as ethene, propene, 1,3-butadiene, and butene isomers. On average, the markedly elevated levels of alkenes contributed more than 50% of the observed OH reactivity over the DPCC (**Figure 3a**). It was notable that the contribution of 1,3-butadiene to the OH reactivity (17%) was the same as that of ethene and propene (17% each). Elevated levels of 1,3-butadiene oxidation products, such as butadiene-HN and APAN, were also observed up to hundreds of pptv (Section 4.2). Alkanes contributed 12% of the OH reactivity followed by the contributions from aromatics (7%), such as benzene, toluene, m,p-xylene, and styrene. The contribution of biogenic compounds including isoprene, isoprene oxidation products (i.e., MVK, MACR, ISOPOOH, and IEPOX), and α, β-pinene to OH reactivity were minimal (less than
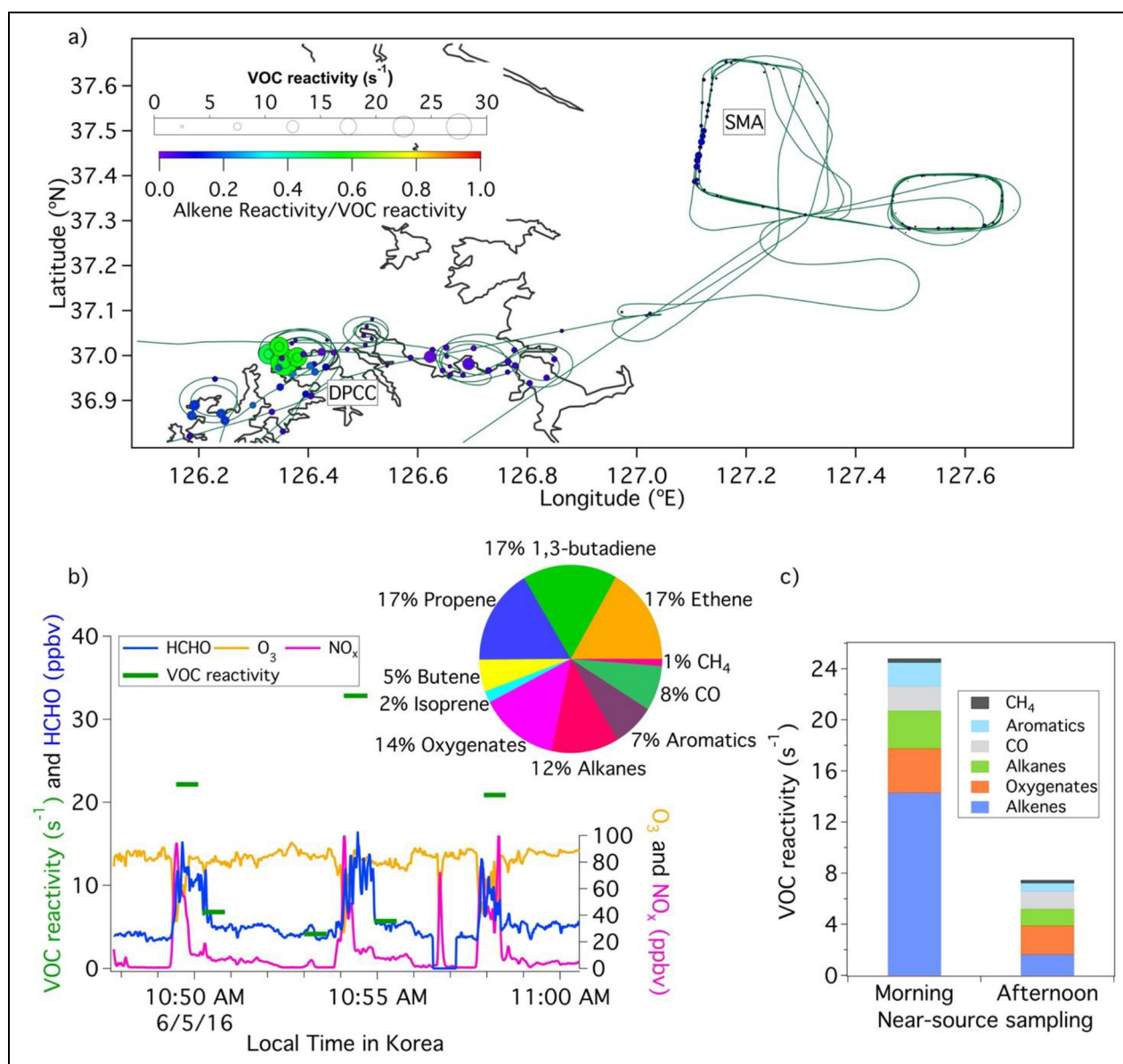
Figure 3. The estimated OH reactivity of volatile organic compounds (VOCs) during RF18. (a) Calculations of the OH reactivity of VOCs over Seoul and Daesan petrochemical complex (DPCC) using the 60s-merged data set. Markers are sized and colored by the OH reactivity of VOCs and the alkene contributions to the OH reactivity of VOCs, respectively. Black lines are the DC-8 flight track during RF18. (b) Time series of 1s measurements of O_3, NO_x, and HCHO and the calculated OH reactivity of VOCs from the near-source DPCC transects during RF18. The relative contributions of speciated VOCs and VOC class to the averaged OH reactivity are shown in the pie chart. (c) The relative contributions of VOC class to the OH reactivity of VOCs in the morning and afternoon transects during RF18.

approximately 6%) over the DPCC. In contrast to the DPCC emissions, aromatics and isoprene contributed to 61% of the averaged OH reactivity over Seoul with lower contribution from nonisoprene alkenes (19%). In addition, Simpson et al. (2020) reported significantly lower levels of 1,3-butadiene (<50 pptv) in both airborne and ground-based measurements in the SMA.

The reactions of alkenes with OH radicals can lead to the formation of oxygenates, such as formaldehyde (HCHO) and acetaldehyde (Ryerson et al., 2003; Wert et al., 2003). In addition, these oxygenates can be directly emitted as by-products of various petrochemical processes (e.g., process emissions and gas flaring). Fried et al. (2020)

and Cho et al. (2021) showed the dominance of secondarily produced HCHO from alkene precursors, such as ethene, propene, butene, and 1,3-butadiene in the observed near-source and downwind DPCC plumes. For the morning plume transects (**Figure 3c**), the contribution of the oxygenates to the calculated OH reactivity was 14%. For the afternoon transects on the same day, **Figure 3c** shows that the average VOC-OH reactivity was a factor of 3 lower than that of the morning transects, suggesting photochemical removal of VOCs in a deeper boundary layer and possible changes in emission characteristics (Fried et al., 2020). While the contribution of alkenes to the OH reactivity (22%) decreased in the afternoon samples, those of
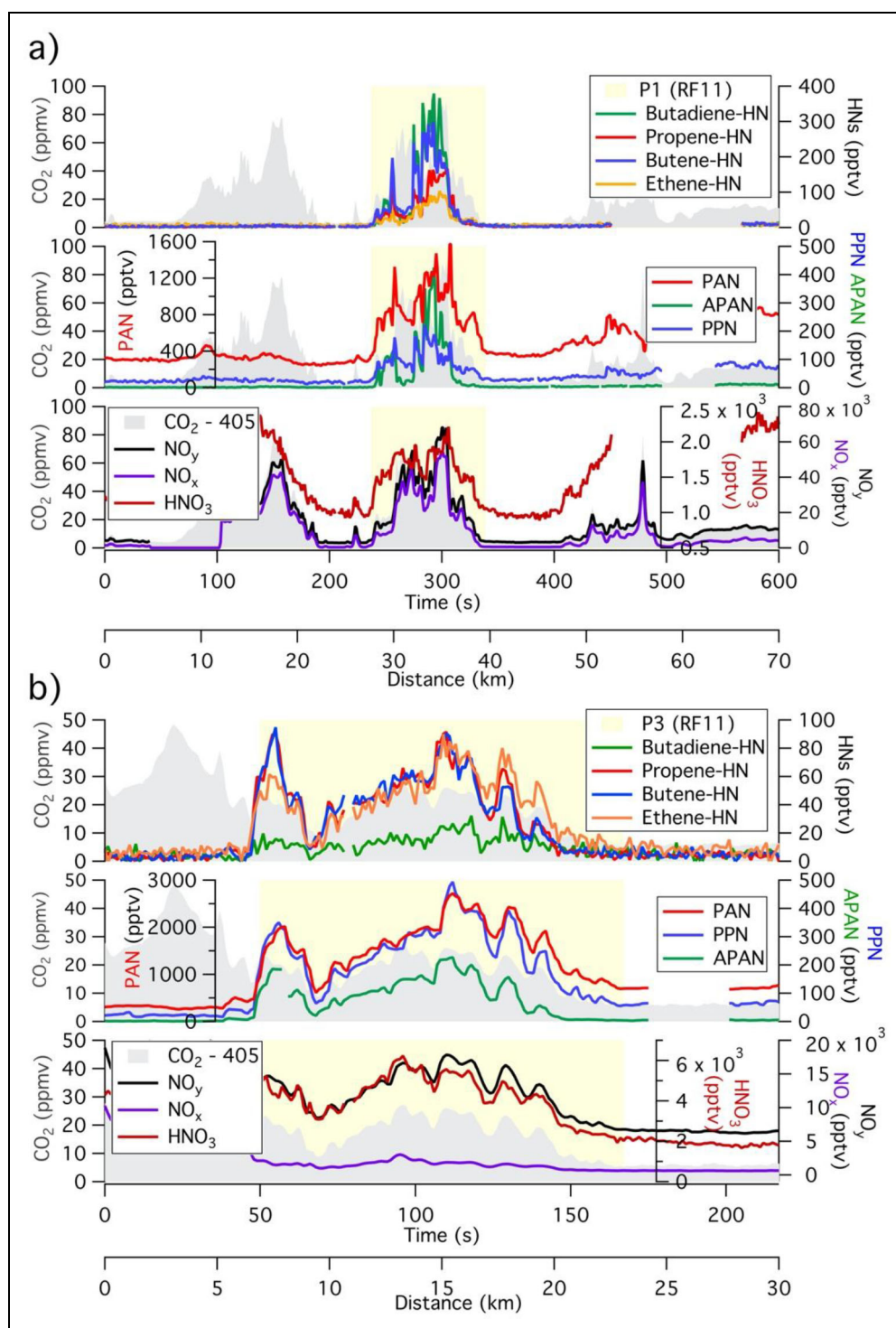
Figure 4. Time series of 1s data of CO_2 and speciated NO_z compounds including HNO_3, PANs, and HNs within (a) fresh plume (P1) and (b) aged plume (P3) transects. Observations of hydroxy nitrates, PANs and NO_y, NO_x, and HNO_3 are illustrated in top, middle, and bottom panel, respectively, of both (a) and (b).

oxygenates increased to 30%, consistent with efficient production of these species from alkene precursors.

4.2. Reactive nitrogen

4.2.1. Observation of reactive nitrogen

Chemical transformation of primary petrochemical emissions of VOCs and NO_x forms oxidation products (NO_z), such as HNO_3, PANs, and ANs (ΣANs) (Ryerson et al., 2003; Neuman et al., 2009). **Figure 4** shows the temporal

changes in the components of NO_y using speciated and total NO_y measurements within P1 and P3, where P1 and P3 are used as an example of relatively fresh and aged downwind DPCC plumes. **Table 2** summarizes the transect average excess mixing ratios of selected NO_y species ($\Delta X = X_{plume} - X_{background}$) along with the background mixing ratios determined based on the average of measurements made 5s before and after the plume encounter. **Figure 4a** illustrates the reactive nitrogen measurements

Table 2. Selected reactive nitrogen mixing ratios measured on May 22, 2016 (RF11) over the Yellow Sea in petrochemical plumes used in this study

	P1			P3		
Compound	Excess Mixing Ratios (pptv)	Background Mixing Ratio (pptv)	$\Delta X/\Delta NO_y$ (pptv pptv^{-1}; %)	Excess Mixing Ratio (pptv)	Background Mixing Ratio (pptv)	$\Delta X/\Delta NO_y$ (pptv pptv^{-1}; %)
NO_y	2.6×10^4	4.0×10^3	–	3.4×10^3	9.0×10^3	–
NO_x	2.2×10^4	9.8×10^2	85	3.4×10^2	1.1×10^3	10
HNO_3	6.0×10^2	1.0×10^3	2.3	1.1×10^3	3.1×10^3	32
PAN	5.2×10^2	3.6×10^2	2	9.7×10^2	6.2×10^2	29
PPN	67	28	0.26	1.7×10^2	62	5
APAN	89	2	0.34	77	16	2.3
Ethene-HN	31	6	0.12	23	17	0.68
Propene-HN	53	4	0.2	22	16	0.65
Butene-HN	84	5	0.32	25	13	0.74
Butadiene-HN	93	4	0.36	6.7	6	0.2

The excess mixing ratios (ΔX) are calculated by subtracting the mixing ratios of X in the background air from those in the Daesan petrochemical complex plume transects P1 and P3 sampled during RF11. NO_x = nitrogen oxides; HNO_3 = nitric acid; PAN = peroxycarboxylic nitric anhydrides; PPN = peroxypropionic nitric anhydride; APAN = peroxyacrylic nitric anhydride; HN = hydroxy nitrate.

in relatively fresh DPCC plumes. Over the plume width of approximately 70 km, the middle plume segment (P1) showed pronounced enhancements of VOCs, NO_x, and NO_z with no significant elevation of CO and SO_2 (Figure S1). This is significantly different than the adjacent plumes with enhanced levels of CO, CO_2, and SO_2 but with minimal enhancements of VOCs, PANs, and HNs (Figure S1; top and middle panels of **Figure 4a**). Within P1, NO_x accounted for 84% of the observed total NO_y, where the sum of NO_x oxidation products (i.e., HNO_3 + PANs + ΣANs) accounted for 8% of the observed NO_y. Further downwind in P3, the contributions of NO_x to NO_y decreased to 10% and the sum of HNO_3, PANs, and ΣANs increased to 82% of NO_y (**Table 2** and **Figure 4b**). For both P1 and P3, the contributions of particulate-NO_3^- to NO_y were consistently 4%.

Fast measurements of speciated reactive nitrogen allow detailed investigations of the photochemistry in evolving petrochemical plumes. For example, measurements of HNs showed strong enhancements within P1 (ΔHNs/$\Delta\Sigma$ANs approximately 32%). In the transect further downwind, the excess HNs mixing ratios decreased and contributed 19% of $\Delta\Sigma$ANs in P3 likely due to the fast oxidation of HNs and their alkene precursors by the OH radical in combination with dilution (Treves and Rudich, 2003; Teng et al., 2015). The strong enhancements of HNs over DPCC are consistent with the large contribution of alkenes to the observed OH reactivity in the DPCC plumes. In particular, butadiene-HN was measured up to 3.8×10^2 pptv and accounted for roughly 30% of the sum of observed HNs, consistent with rapid production from oxidation of 1,3-butadiene.

Another example of photochemistry leading to unique reactive nitrogen processing in petrochemical plumes is illustrated in PAN and PAN homologue (PANs) measurements (Roberts et al., 2001; Roberts et al., 2003). Enhancements of PAN, usually the dominant PANs compound (>80% of PANs) (Roberts et al., 2007), was less than half of the sum of PANs within P1. The reduced contribution of PAN has been observed in oil and natural gas and petrochemical producing regions (Roberts et al., 2003; Lindaas et al., 2019; Lee et al., 2021). In P1, APAN was measured up to 4.3×10^2 pptv with concurrent enhancements of butadiene-HN. The campaign maximum APAN level (8.5×10^2 pptv) was observed over the Yellow Sea during RF18 (Table S5). Within petrochemical plumes, significantly elevated levels of APAN were comparable or often higher than those of peroxypropionic nitric anhydride (PPN), which is usually the second most common PAN compound in urban environments (PPN/PAN approximately 10%–15%). Table S5 and Figure S3a summarize PANs measurements and locations during the KORUS-AQ campaign. **Figure 5a–c** shows the relationship between observed O_x (O_3 + NO_2) and PANs during RF11, where the gray markers represent the measurements outside the DPCC plumes. The observed O_x was only correlated with APAN within petrochemical plumes in contrast to the consistent positive relationship of O_x with PAN and PPN due to a wide range of hydrocarbon precursors that can form PAN and PPN as well as ozone. Similarly, Figure S3b shows that APAN is much higher over the DPCC compared to other regions in Korea in contrast to a more uniform distribution of PAN, PPN, and HCHO. This is consistent with our experience from previous airborne field
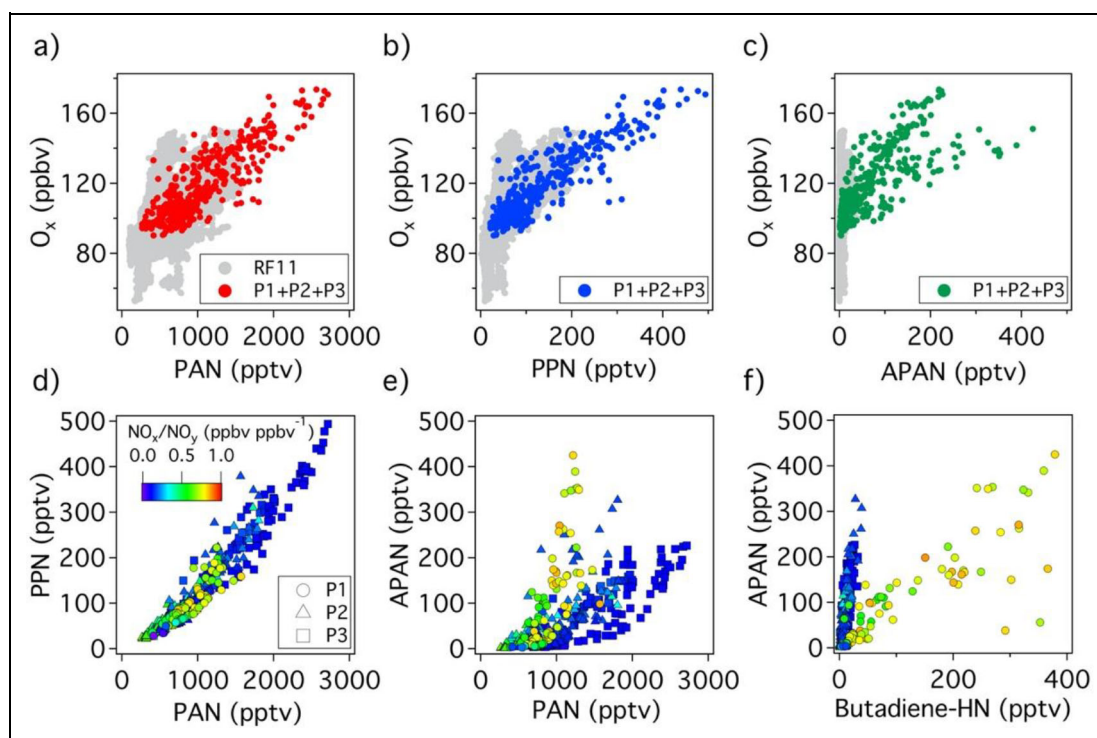
Figure 5. The observed relative abundance among O$_x$, PANs, and butadiene-HN during RF11. Scatter plots of the regression of O$_x$ versus (a) PAN, (b) PPN, and (c) APAN. The colored and gray markers represent the DPCC plume transects (P1–P3) and measurements outside the DPCC plumes, respectively. Scatter plots of the regression of (d) PPN and (e) APAN versus PAN, and (f) APAN versus Butadiene-HN for P1 (circles), P2 (triangles), and P3 (squares) colored by NO$_x$/NO$_y$ ratios. PAN = peroxycarboxylic nitric anhydrides; PPN = peroxypropionic nitric anhydride; APAN = peroxyacrylic nitric anhydride; HN = hydroxy nitrate; DPCC = Daesan petrochemical complex.

campaigns, including the Studies of Emissions and Atmospheric Composition, Clouds and Climate Coupling by Regional Surveys (SEAC⁴RS; Liu et al., 2016; Liu et al., 2017) and the Fire Influence on Regional to Global Environments of Air Quality (Bourgeois et al., 2022), where high APAN levels were only observed in petrochemical and biomass burning plumes. In addition, **Figure 5d** and **e** shows the observed PPN and APAN as a function of PAN in the plume measurements (P1 + P2 + P3) during RF11, where the data points are colored by NO$_x$/NO$_y$ ratios to illustrate changes in the degree of photochemical processing in the sampled airmasses. While the slope of PPN versus PAN is consistently within the range of 0.1–0.2, that of APAN versus PAN decreased with decreasing NO$_x$/NO$_y$ from P1 to P3. This is as expected because reaction with OH is an important loss process for APAN but negligible for PAN and PPN. **Figure 5f** shows that the slope of APAN over butadiene-HN increased from 1 to 6, which is consistent with more efficient loss of butadiene-HN by reaction with the OH radical than APAN ($k_{OH + butadiene-HN}/k_{OH + APAN} \sim 2$) (Orlando and Tyndall, 2002; Treves and Rudich, 2003). In addition, butadiene-HN is formed in the earlier stage of 1,3-butadiene oxidation at higher NO/NO$_2$ conditions, whereas the decrease of NO/NO$_2$ ratios further downwind may increase the slope of APAN/butadiene-HN by decreasing the probability of peroxy radical (RO$_2$) reacting with NO (e.g., Equation 4) and thus increase production and the effective lifetime

of APAN (Sprengnether et al., 2002; Jaoui et al., 2014). The evolution of short-lived reactive nitrogen species is discussed in detail in Section 4.5.2.

During KORUS-AQ, APAN and butadiene-HN often showed concurrent enhancements over the DPCC and the Yellow Sea, suggesting APAN is formed primarily from the oxidation of 1,3-butadiene in this environment. Significant enhancements of APAN and HNs including butadiene-HN were also observed outside of the DPCC over the South Sea on May 7, 2016, when northwesterly wind transported pollution from coastal cities such as Ulsan and Busan over the ocean (Figure S4). The observed elevations of APAN and HNs over the South Sea are likely influenced by another major petrochemical complex, the Ulsan Petrochemical Complex, with an ethene production capacity half that of the DPCC. Therefore, the elevated levels of APAN and HNs during the KORUS-AQ illustrate the impact of local petrochemical sources such as the DPCC and the Ulsan Petrochemical Complex on atmospheric photochemistry.

4.2.2. Investigation of petrochemical plume chemistry utilizing PANs measurements

Here, we utilize APAN as a photochemical tracer to investigate petrochemical plume chemistry due to its relatively short lifetime and low background levels with a clear enhancement in petrochemical plumes. **Figure 6a** and **b** shows the regression of observed ozone and
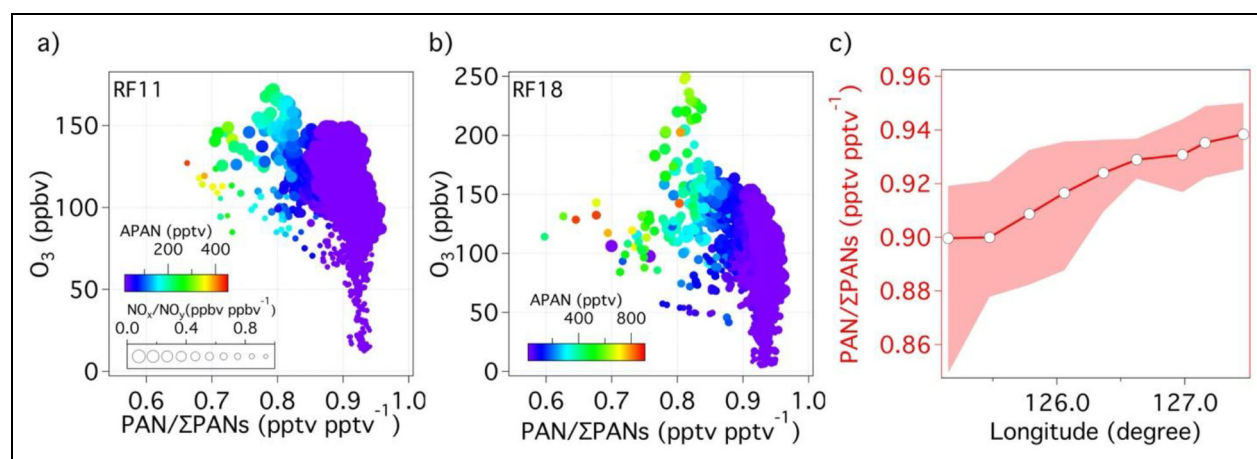
Figure 6. Scatter plots of the regression of O_3 versus PAN/ΣPANs colored and sized by APAN mixing ratios and NO_x/NO_y ratios, respectively, during (a) RF11 and (b) RF18, and (c) PAN/ΣPANs using 1s-merged dataset of all Korea-United States Air Quality measurements sampled <500 m. Markers represent bin-averaged PAN/ΣPANs at 0.3 longitude resolution with shaded area indicating 10th and 90th percentile. The longitudes of Seoul and Daesan petrochemical complex/Yellow Sea are approximately 127.1° and <126.2° East, respectively. PAN = peroxycarboxylic nitric anhydrides; APAN = peroxyacrylic nitric anhydride.

PAN/ΣPANs during RF11 and RF18, where PAN/ΣPANs is the relative contribution of PAN to the sum of PAN compounds (i.e., PAN + PPN + APAN) measured by the GT-CIMS. The markers are 1s-merged data that are color-coded and sized using APAN mixing ratios and NO_x to NO_y ratios, respectively. Again, NO_x to NO_y ratios provide a proxy of photochemical processing. On average, higher ozone levels were observed in airmasses with lower NO_x/NO_y. The observed ozone levels increased with decreasing PAN/ΣPANs, suggesting oxidation of anthropogenic hydrocarbons leading to the production of PAN homologues such as PPN and APAN as well as that of ozone. For both RF11 and RF18, the highest elevated levels of ozone were observed with larger contributions of APAN to ΣPANs (i.e., decreasing PAN/ΣPANs) within the DPCC plumes. The highest levels of APAN were observed with moderate ozone levels in young petrochemical plumes. In contrast to the larger contribution of PPN and APAN in petrochemical plumes, bin-averaged PAN/ΣPANs at 0.3° longitude resolution were larger over Seoul than the DPCC illustrating the dominance of PAN in the urban environment (**Figure 6c**).

Similar results were observed during TexAQS-2006 study, where Zheng et al. (2007) observed higher ozone to PAN ratios in petrochemical plumes (approximately 19) than in urban and power plant plumes (approximately 12–15). The elevated O_3/PAN ratios were attributed to the oxidation of ethene and 1,3-butadiene producing ozone but not PAN. However, the role of such reactive alkenes on ozone production and reactive nitrogen processing in petrochemical plumes may be more complex if oxidation of such compounds leads to formation of additional peroxy nitrates (PNs) other than PAN (e.g., APAN), which can sequester NO_x. For example, another heavily polluted atmospheric environment with significant levels of VOCs and NO_x is biomass burning plumes, where heterogeneity in VOCs emissions, especially oxygenated VOCs, together

with NO_x makes accurate descriptions of fire plume chemistry challenging. A recent analysis by Wolfe et al. (2022) shows that incorporating more VOCs in model simulations for wildfire plumes can lower ozone and PAN due to the formation of larger PNs during oxidation of acrolein, glycolaldehyde, and other VOCs. The photochemical evolution of petrochemical emissions is also likely to be complex. In part, this complexity is reflected by the markedly higher abundance of APAN as well as HNs in the petrochemical plumes relative to the other environments observed during the KORUS-AQ. For this reason, we further investigate effects of reactive alkenes on ozone production and reactive nitrogen processing in petrochemical plumes in subsequent sections utilizing in situ observations and a model case study.

4.3. Ozone production in DPCC plumes
4.3.1. Instantaneous ozone production rates
The instantaneous ozone production rate $P(O_3)$ and OPE were estimated using the methods described in Section 3.2. **Figure 7a** on the left axis shows the sum of the averaged contributions from individual hydrocarbons to ozone formation for selected petrochemical plume transects. The estimated average $P(O_3)$ was 19 ± 3 (1σ) ppb h^{-1} and 8.8 ± 1.8 (1σ) ppb h^{-1} for P1 and P3 from RF11, respectively. Figure S5 shows the relative contributions of the VOC class to $P(O_3)$. In the young plume (P1), alkenes contributed 39% of the total calculated $P(O_3)$, followed by the contribution from oxygenates (38%), alkanes (14%), aromatics (5%), CO (3%), and CH_4 (1%). The contribution from alkenes decreased to 7% in P3, while the oxygenates account for 56% of the averaged $P(O_3)$. For RF18, where the measurements include both near-source and downwind DPCC plume samples, the dominance of oxygenates to $P(O_3)$ was observed in the downwind DPCC plumes. For example, P4 with an estimated transport time of approximately 2.5 h (Fried et al., 2020) was sampled around
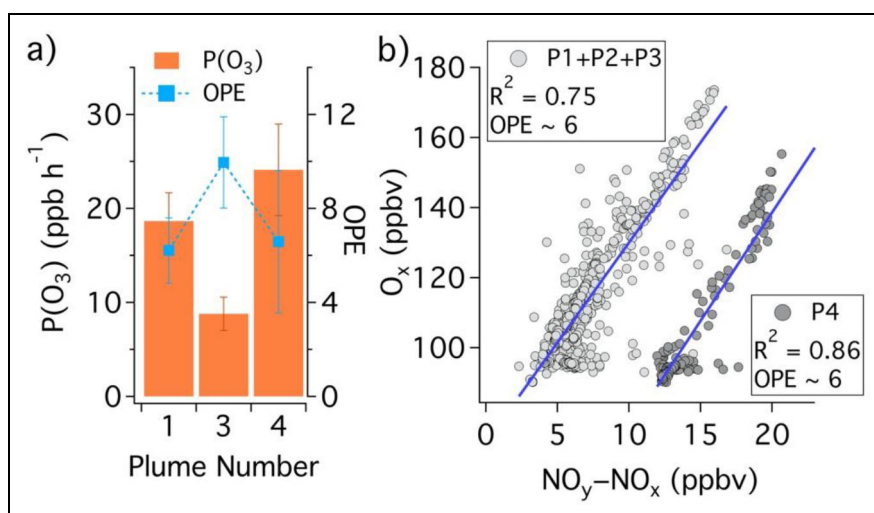
Figure 7. The estimated ozone production rate and efficiency. (a) Instantaneous $P(O_3)$ (left axis) and ozone production efficiency (OPE; right axis) for the selected Daesan petrochemical complex plumes. (b) Empirical OPEs determined based on the regression of the observed O_x versus NO_z ($NO_y - NO_x$) during RF11 (P1 + P2 + P3) and RF18 (P4).

noon and had the highest $P(O_3)$ value, 24 ± 5 (1σ) ppb h^{-1}, during RF18. For P4 from RF18, the oxygenates contributed 55% of the total $P(O_3)$ followed by alkanes (16%) and alkenes (13%).

On average, the calculated $P(O_3)$ at low altitude (<500 m) was markedly higher over the DPCC and the Yellow Sea than that over Seoul during RF11 and RF18 (Figure S6). $P(O_3)$ including all samples (petrochemical and nonpetrochemical) collected over the DPCC and the Yellow Sea ranges from 1.7 to 24 ppb h^{-1}. In contrast, $P(O_3)$ over Seoul was in the range of 1.8–7.8 ppb h^{-1}. Compared to the model estimated $P(O_3)$ over Seoul during the KORUS-AQ by Schroeder et al. (2020), the estimated range of $P(O_3)$ in this study is in a reasonable accord with the column-average values of modeled $P(O_3)$ that ranged from 3.2 to 7.5 ppb h^{-1}. In addition to the higher $P(O_3)$ over the DPCC relative to Seoul, there was a large difference in the contributions of the VOC class to $P(O_3)$. Both the observed OH reactivity for Seoul and the model sensitivity analysis by Simpson et al. (2020) and Schroeder et al. (2020), respectively, illustrated large contribution of aromatics (approximately 45%) and isoprene (approximately 20%) to ozone production in Seoul, whereas these compounds only made minor contributions (<6%) to the calculated $P(O_3)$ in the DPCC plumes.

4.3.2. Instantaneous and empirical OPE
Figure 7a also shows the instantaneous OPE for the selected petrochemical plumes. The average instantaneous OPEs for the DPCC plumes range from 6 to 10. The highest value was found in the relatively mature plume (P3). This is consistent with a decrease in the observed NO_x to NO_y ratios from 0.7 to 0.1 ppb ppb^{-1} from P1 to P3 (Figure S2), as the higher levels of NO_x to VOCs levels early in the plume limit ozone production due to radical loss by HNO_3 production. In general, the instantaneous OPEs over the DPCC and the Yellow Sea were lower than 15 and were not

significantly different compared with those over Seoul (from 2 to 15) (Figure S6). This indicates the elevated $P(O_3)$ over the DPCC and the Yellow Sea was balanced by fast formation of HNO_3 and PAN.

Figure 7b shows the empirical OPEs estimated from the slope of regression plots between the observed O_x and NO_z. The empirical OPE represents the integrated results from the production and loss process of ozone and NO_z in the atmosphere. For selected petrochemical plumes during RF11 and RF18, the empirical OPEs were approximately 6, which fall within the estimated range of the instantaneous OPEs. Although it is difficult to derive the integrated OPE for Seoul based on the observed regression of O_x over NO_z due to complicated source emissions and varying background levels, the O_x/NO_z ratios over Seoul based on the linear regression were generally less than 10. The OPEs in Seoul have been reported by Kim et al. (2020) and Oak et al. (2019) using ground-based measurement at the Olympic Park Site, in the center of SMA, and model simulations, respectively. The OPE derived from the ground-based measurements of O_x and NO_z ($NO_y - NO_x$) ranged from 3.1 to 6.3 for daytime conditions (Kim et al., 2020). In addition, the modeled spatial distribution of instantaneous OPEs by Oak et al. (2019) showed that OPEs are generally lower than 10 for Seoul and industrial areas along the west coast, in which DPCC and other industrial facilities are located, in contrast to the higher OPEs (10–30) in rural areas.

4.4. Potential SOA production rate
The contribution of individual VOCs to the instantaneous SOA production rate, P(SOA), was estimated using the method described in Section 3.3 and the parameters illustrated in Figure S7. **Figure 8** shows P(SOA) and the fractional contributions of speciated VOCs to P(SOA) for selected DPCC plume transects. Within P1, aromatics (56%) made the largest contribution to P(SOA) (0.97 µg
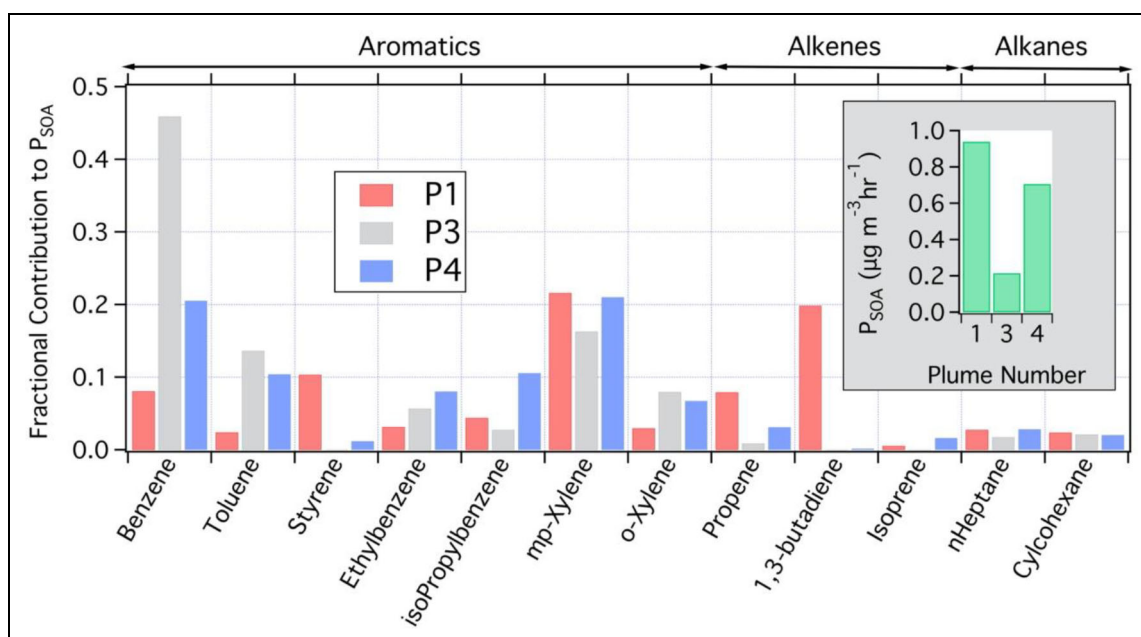
Figure 8. Fractional contributions of the speciated volatile organic compounds (VOCs) to P(SOA). The inset shows the values of P(SOA) for the selected plume transects. Note that P1 and P3 are from RF11 and P4 from RF18.

$m^{-3} hr^{-1}$), followed by alkenes (35%) and alkanes (7%), where the oxidation of hydrocarbons was by reaction with the OH radical (92%) and O_3 (8%). In particular, reactive aromatics, such as xylenes and styrene, were the most important aromatic precursors of SOA accounting for approximately 30% of the calculated P(SOA). For transects further downwind from the DPCC (P3), the contributions of small alkenes were minimal (1%). Instead, P(SOA) was dominated by aromatics (94%), such as benzene, toluene, and xylenes, with contributions from alkanes (5%).

The appreciable fractions of P(SOA) from small alkenes such as propene (8%) and 1,3-butadiene (20%) at intermediate distances (approximately 30 km) from the DPCC (P1) were comparable to those of aromatics, which are important SOA precursors in Seoul and other urban environments (Nault et al., 2018, and references therein). This suggests the potential importance of small alkenes ($<C_{11}$), in not just ozone formation, but in ambient SOA formation in petrochemical plumes, especially at earlier photochemical ages when such compounds contribute significantly to OH reactivity. This is in contrast to previous studies where the contribution of alkenes to SOA formation is thought to be minimal in petrochemical plumes due to the high volatility of their oxidation products (Bahreini et al., 2009; Wood et al., 2010). For example, Wood et al. (2010) assumed that yields from alkenes are negligible besides isoprene in the calculation of P(SOA) using a method similar to this work. This led to approximately a factor of 2 higher P(SOA) to P(O$_x$) ratios for Mexico City (2–48 μg m^{-3} ppmv^{-1}) than those for Houston (1–26 μg m^{-3} ppmv^{-1}), where the smaller P(SOA)/P(O$_x$) for Houston was caused by a significant portion of P(O$_x$) attributed to small alkenes. The P(SOA) to P(O$_x$) ratios of the selected DPCC plumes in **Figure 8** ranged from 24 to 50 μg m^{-3} ppmv^{-1}. When the upper ends are compared, our values

were comparable and a factor of 2 higher than the value for Mexico City and Houston, respectively. The higher P(SOA)/P(O$_x$) estimated in this work can be explained by the use of the updated parameters from Ma et al. (2017) accounting for vapor wall loss to derive SOA yields of alkenes (0.03–0.09 at [OA] approximately 20 μg m^{-3}) as well as a factor of approximately 3 higher AN branching ratios (Teng et al., 2015), which have been reevaluated since Wood et al. (2010).

Nault et al. (2018) utilized similar methods to derive SOA yields (Ma et al., 2017) over the SMA. They attributed the majority of SOA production in the SMA to toluene (9%) and short-lived aromatics (70%), such as ethyltoluenes, trimethylbenzenes, and xylenes. In comparison, most short-lived aromatics were insignificant SOA precursors for the DPCC plumes, except m,p-xylene which contributes approximately 20% of P(SOA). The most important DPCC emissions for local SOA production are m,p-xylene, l,3-butadiene, and styrene accounting for 52% at P1. Nault et al. (2018) also found in the SMA that OA was strongly correlated to PAN ($r^2 = 0.7$) and aromatic oxidation products such as dihydroxytoluene ($r^2 = 0.41$), consistent with local SOA production over Seoul from a wide range of VOC dominated by aromatics. However, in the DPCC at P1 the observed OA correlated more strongly with HCHO, APAN, and butadiene-HN (Figure S8a–c), secondarily produced from alkene precursors, than PAN, dihydroxytoluene, and benzaldehyde (Figure S8d–f). In addition to the different SOA precursors in the DPCC and the SMA, the strong correlations of OA with alkene oxidation products suggest that DPCC SOA production may be markedly different to the SMA.

The potential importance of anthropogenic small alkenes in SOA formation has been discussed in several laboratory and field studies. The empirical SOA yields for

propene (Ge et al., 2017) and 1,3-butadiene (Sato et al., 2011) from chamber experiments were a factor of approximately 5 lower than and comparable to the values used in this work, respectively, but much greater than those in Wood et al. (2010) (Figure S9). Ge et al. (2017) attributed SOA formation from propene to aqueous-phase reaction of propene oxidation products in the presence of aerosol water, where the importance of aqueous-phase reaction for SOA formation from other VOCs with relatively lower molecular weight (e.g., ethene and ethyne) has been demonstrated by previous studies (Volkamer et al., 2009; Huang et al., 2011; Jia and Xu, 2016). However, the SOA yield from propene in this work may be overestimated due to relative humidity levels lower than that in Ge et al. (2017) despite similar OA concentrations and temperature. For 1,3-butadiene oxidation in high NO_x conditions, Sato et al. (2011) showed that the measured SOA yield for 1,3-butadiene oxidation (0.089–0.178) was similar or slightly higher than that measured for isoprene oxidation (0.077–0.103) in similar experimental conditions (i.e., OA concentrations, temperature, and j-NO_2) as observed in the DPCC plumes. The SOA yields of 1,3-butadiene in the parametrization by Ma et al. (2017) were also higher than other alkenes including isoprene. Detailed investigations of gas phase and particulate phase composition in laboratory and field samples by Jaoui et al. (2014) suggest that oxygenated organic compounds (e.g., glyoxal, glycolaldehyde, glyceric acid, threitol, and APAN) from 1,3-butadiene oxidation can contribute to ambient SOA formation in regions with large 1,3-butadiene emissions. The experimental investigation of small alkene oxidation on the observed OA mass in the DPCC plumes is difficult and beyond the scope of this work. This is in part due to the ambient processes governing loss of aerosol and the role of alkene oxidation on photochemical conditions (e.g., oxidant levels), which can complicate SOA production in a mixture of different hydrocarbon precursors and NO_x. Instead, we demonstrate nonnegligible contributions of alkenes, such as propene (8%) and 1,3-butadiene (20%), to our simple calculation of P(SOA) due to their high reactivity and large abundance in petrochemical plumes at intermediate distances. For this reason, we suggest that the small alkenes, such as propene and 1,3-butadiene, are not only important in local production of ozone but also of SOA. In future studies, a detailed investigation of petrochemical plumes, which has a significant abundance of alkenes with NO_x, may provide a useful test bed to understand the impacts of small alkenes on ambient SOA formation.

4.5. Model case study

We investigate the chemical evolution of petrochemical plumes utilizing a model case study with a suite of observational constraints from the DC-8 payload and a near-explicit model mechanism (MCM). To study the potential impacts of reactive VOCs and other radical precursors on the evolution of O_3 and reactive nitrogen, we focus on the evolution of short-lived reactive nitrogen such as PANs and HNs, which provides a useful diagnostic of model-simulated oxidation process in an example petrochemical plume.

Figure 9 shows the observed and modeled mixing ratios of the selected trace gases, where the observed plume mixing ratios are transect-averages of P1–P3 after filtering out data with APAN levels lower than 50 pptv to exclude data measured outside the DPCC plumes. The plume transport time is estimated based on the distance of the plume transects from the DPCC divided by the average wind speed of 4 m s^{-1}. For the modeled dilution process, **Figure 9a** shows the simulated CO_2 mixing ratios using the dilution parameter (k_{dil}) with τ_{gauss} chosen to best fit the observed CO_2 mixing ratios from the selected plume transects. This is illustrated along with the simulated CO_2 using one half of τ_{gauss} and twice τ_{gauss} to investigate the impact of faster and slower dilution (i.e., higher and lower k_{dil} according to Equation 7, respectively) on the plume evolution.

4.5.1. Ozone

Figure 9a shows the simulated and observed mixing ratios of ozone. The simulated O_3 mixing ratios were in reasonable accord with the observed O_3 mixing ratios. The model captures the observed decrease in downwind NO/NO_2 ratios well. **Figure 9b** shows the simulated ozone production rate, P(O_3), determined by the sum of the rates of reaction of HO_2 and RO_2 with NO. The simulated ozone production rate agreed well with the instantaneous ozone production rates calculated in Section 4.3.1 to within approximately 10% in general. The simulated P(O_3) decreased over the model integration time due to rapid decrease in the concentrations of VOCs and NO_x, and a similar trend is observed in the decrease of instantaneous P(O_3) from P1 to P3. The relative contribution of VOCs to ozone production was investigated using zero-out sensitivity tests, where the concentrations of each VOC class were set to zero (e.g., Schroeder et al., 2020). The simulated P(O_3) decreased by 66% and 9% without initial constraints of alkenes and aromatics, respectively. This is consistent with more than 70% of the observed OH reactivity and instantaneous P(O_3) attributed to alkenes and oxygenates. To quantify how efficiently ozone is produced, we calculated OPE by dividing P(O_3) by the production rates of NO_x oxidation products (e.g., $NO_z \equiv$ HNO_3, PNs, and ANs). **Figure 9c** shows that the simulated OPE achieved maximum efficiency downwind with decreasing rates of NO_z production, where this downwind evolution of OPE was also illustrated by an increase in the instantaneous OPE from P1 to P3. On average, the model-simulated ozone production is consistent with observations.

4.5.2. Short-lived reactive nitrogen

The simulated and observed mixing ratios of the selected reactive nitrogen are shown in **Figure 9d** and **e**. The model reproduced the observed levels of PANs and HNs reasonably well. In particular, the model was more successful in reproducing the enhancements and evolution of APAN and HNs than PAN likely due to a limited range of precursors and lower and less variable background levels. The simulated APAN and butadiene-HN show a reasonable agreement with the observed levels, indicating that
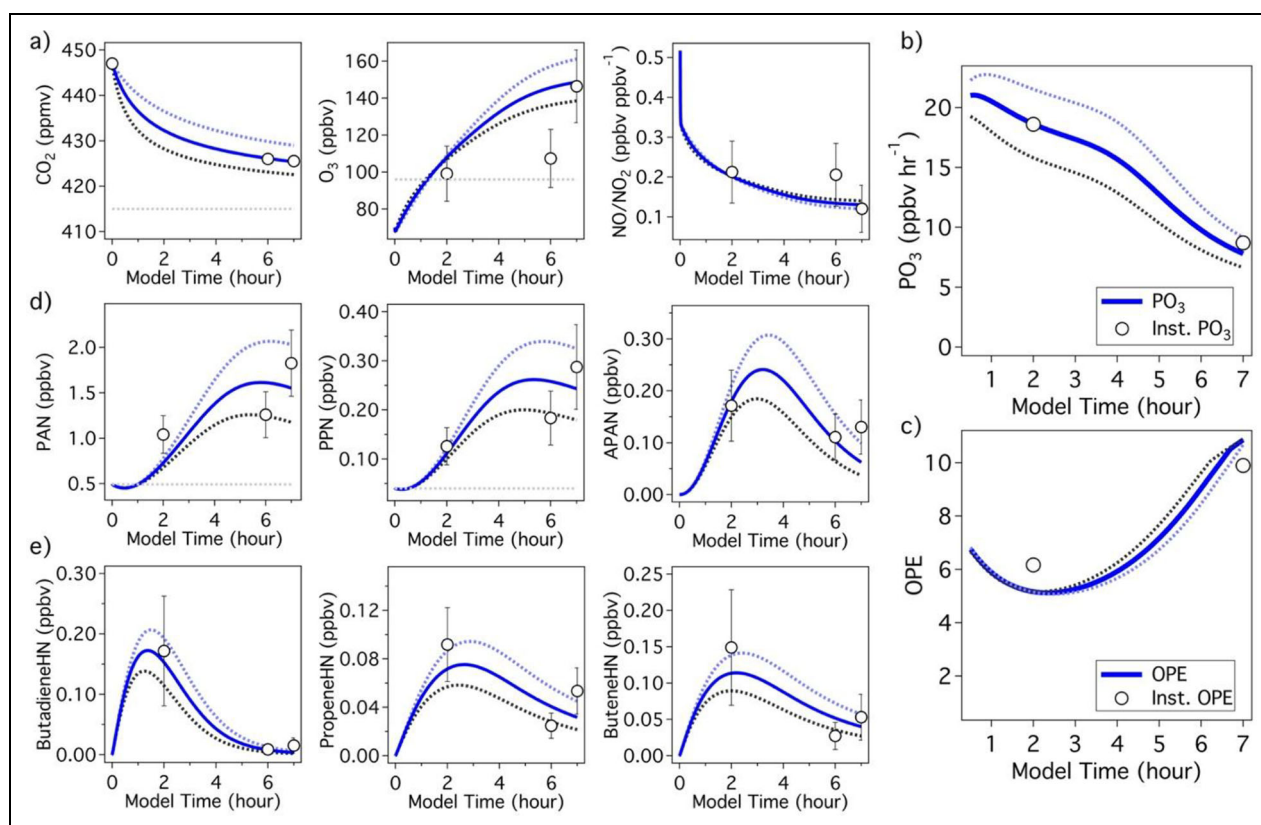
Figure 9. The diagnostic model simulations of the selected primary and secondary species along with the model prediction of ozone production rate and ozone production efficiency (OPE). The model simulated results of (a) CO_2, O_3, and NO/NO_2, (b) $P(O_3)$, (c) OPE, (d) PAN, PPN, and APAN, and (e) butadiene HN, propene HN, and butene HN over 7-h model integration time. The solid blue lines, cyan dashed lines, and black dashed lines correspond to the base case, slower dilution case, and faster dilution case, respectively. The gray horizontal dashed line indicates background mixing ratios used for model input. The open circles represent the averages of the DPCC plumes transects (P1–P3), where the vertical error bars are measurements uncertainties. PAN = peroxycarboxylic nitric anhydrides; PPN = peroxypropionic nitric anhydride; APAN = peroxyacrylic nitric anhydride.

production of APAN and butadiene-HN was accounted for by the oxidation of 1,3-butadiene. This is corroborated by the rapid oxidation of 1,3-butadiene and production of acrolein in the model, although it was notable that the model underestimated the butadiene level at P1, consistent with the higher modeled OH than the observations (Figure S10). In addition, uncertainty in both plume ages and plume observations of butadiene, due to the limited time response of the measurement, may contribute to the discrepancy. On average, the efficient conversion of NO_x to the short-lived reactive nitrogen species followed by the later decay due to reaction with OH indicates the impacts of reactive VOCs, especially alkenes, on the production and distribution of reactive nitrogen throughout the plume evolution. In these plumes, species such as PANs and HNs can be a temporary sink or source of radical and NO_x that modulate photochemistry at different stages of downwind plume evolution.

The model outputs also include additional PNs that are not measured by the DC-8 payload. Notably, these unmeasured PNs contribute approximately 30% of the model-simulated PNs budget shown in **Figure 10**. The contribution of PAN and PPN was approximately 60% of the PNs budget at 7 h of model integration. This is in contrast to previous observations of typical urban plumes, where PAN and PPN are a larger fraction of the PNs budget (>80%) (Roberts et al., 2007; Wooldridge et al., 2010). The contribution of APAN was 14% and 2% at 2 and 7 h of the model integration time, respectively. Among the unmeasured PNs, peroxyhydroxyacetic nitric anhydride (PHAN) and peroxybenzoic nitric anhydride (PBzN) were estimated to contribute 17% and 6% to the predicted PNs budget, respectively. The aldehyde precursor for PHAN is glycolaldehyde, and for PBzN is benzaldehyde. Although these aldehydes can be emitted, glycolaldehyde can be produced from oxidation of anthropogenic and biogenic VOCs including ethene, 1,3-butadiene, and isoprene. Benzaldehyde can be produced from reactive aromatics including toluene, styrene, and other aromatic compounds. To investigate the impacts of these VOCs precursors on the modeled PNs budget, zero-out sensitivity tests without the initial model constraints of speciated and classes of VOCs were performed. PHAN, PBzN, and APAN were almost exclusively formed from the oxidation of ethene and 1,3-butadiene, styrene, and 1,3-butadiene, respectively, in the MCM (Figure S11). In contrast, PAN and PPN were markedly decreased without initial constraints of alkenes, whereas removing alkanes and aromatics also resulted in
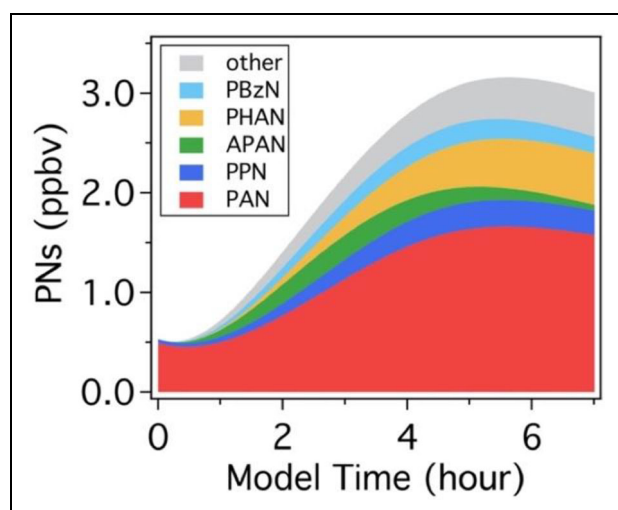
Figure 10. The model simulated budgets of peroxy nitrates in the base case model scenario over a 7-h model integration time.

a decrease in PAN and PPN to a lesser extent. Consequently, the zero-out simulations are consistent with our conclusion that reactive VOCs such as alkenes and styrene have a strong impact on the production and distribution of reactive nitrogen in petrochemical plumes. Since both 1,3-butadiene and styrene are widely used in the petrochemical industry to make products such as a styrene–butadiene–styrene polymer, PHAN and PBzN may be found in petrochemical plumes along with APAN. This is supported by the observed mixing ratios of glycolaldehyde and benzaldehyde up to 8.4×10^2 pptv and 2.1×10^3 pptv within the DPCC plumes by CIT-CIMS and PTR-MS, where these compounds showed enhancements with acetaldehyde, acrolein, and APAN over the Yellow Sea (Figure S12a and b). In our model, the simulated glycolaldehyde and benzaldehyde showed a reasonable agreement with observations when compared to the peak value and average value of earlier DPCC plume transects, respectively, but the simulated glycolaldehyde was higher by up to a factor of approximately 2 than observations at later transects potentially due to neglecting heterogenous loss (Figure S12c and d). In addition, APAN was the second largest contributor to PNs in the first few hours after emission. However, reaction of APAN with OH produces glycolaldehyde and NO_x in the MCM; thus, the oxidation of APAN further facilitates PHAN and/or ozone production. In contrast to the decomposition of APAN in the MCM, several laboratory studies proposed a mechanism by which the APAN-OH adduct leads to aerosol-phase products during the oxidation of 1,3-butadiene and acrolein in the presence of NO_x, which limits the formation of radical precursors from the OH oxidation and thermolysis of APAN (e.g., Chan et al., 2010; Jaoui et al., 2014).

The significant contribution of unmeasured PNs including PHAN and PBzN to the model PNs budget suggests their potentially large abundance in petrochemical plumes and possibly in other polluted VOC-NO_x environments. The potential abundance of PHAN and PBzN may be partially responsible for the OPE of petrochemical

plumes being similar to urban plumes (Neuman et al., 2009) despite significant levels (>tens ppbv in total) of reactive VOCs such as ethene, 1,3-butadiene, and styrene that do not produce PAN. In other words, the production of reactive nitrogen from the oxidation of ethene, 1,3-butadiene, and styrene not only contributes to the radical formation (i.e., ozone production) but also sequester radicals and NO_x by producing reactive nitrogen such as PHAN and PBzN. Laboratory studies have demonstrated the presence of the PHAN and PBzN during the oxidation of glycolaldehyde and benzaldehyde (Fung and Grosjean, 1985; Niki et al., 1987; Zheng et al., 2011), respectively, but there are a limited number of field observations for PBzN (Meijer and Nieboer, 1978; Fung and Grosjean, 1985; Lee et al., 2021) and no ambient measurements for PHAN. Zheng et al. (2011) pointed out the possible loss of PBzN on Teflon inlet wall during the characterization of a TD-CIMS for PANs measurements, indicating the potential to underestimate PBzN levels during KORUS-AQ and other previous ambient measurements. In addition, Zheng et al. (2011) observed the fast loss of PHAN in the FTIR chamber at room temperature and proposed unimolecular thermal decomposition of PHAN that does not produce peroxy radicals to explain the inability to detect PHAN with the TD-CIMS method. The proposed mechanism for PHAN thermolysis also suggests that the MCM may overestimate the simulated PHAN levels. The model sensitivity analysis incorporating the unimolecular decomposition of PHAN decreased the simulated PHAN levels by approximately 70%, but the contribution of PHAN to the simulated PNs was still comparable to that of PPN. In addition, the effect of the unimolecular reaction may be greater if PHAN has a faster thermal decomposition than PAN as suggested by Niki et al. (1987) and Zheng et al. (2011), which might enhance overestimation of PHAN by the model.

The reasonable agreement between the simulated and observed short-lived reactive nitrogen compounds suggests that the model-simulated photochemistry is likely representative of the oxidation process in petrochemical plumes. The simulated rates and efficiency of ozone production agreed reasonably well with our estimations based on the observations. Investigation of the simulated PNs budget points out the potential contributions of rarely measured PAN homologue such as PHAN and PBzN and illustrates the unique photochemistry in petrochemical plumes.

4.6. Comparison with previous studies
We compare the results in this work with previous airborne observations conducted in the Houston area during the TexAQS 2000/2006 and the SEAC[4]RS campaigns.

Observations in the Houston area showed that elevated levels of small alkenes with NO_x were a persistent feature of plumes emanating from local petrochemical facilities in the HSC. Within the HSC plumes, ethene and propene contributed more than 80% of the observed OH reactivity (>15 s^{-1}) (Ryerson et al., 2003).

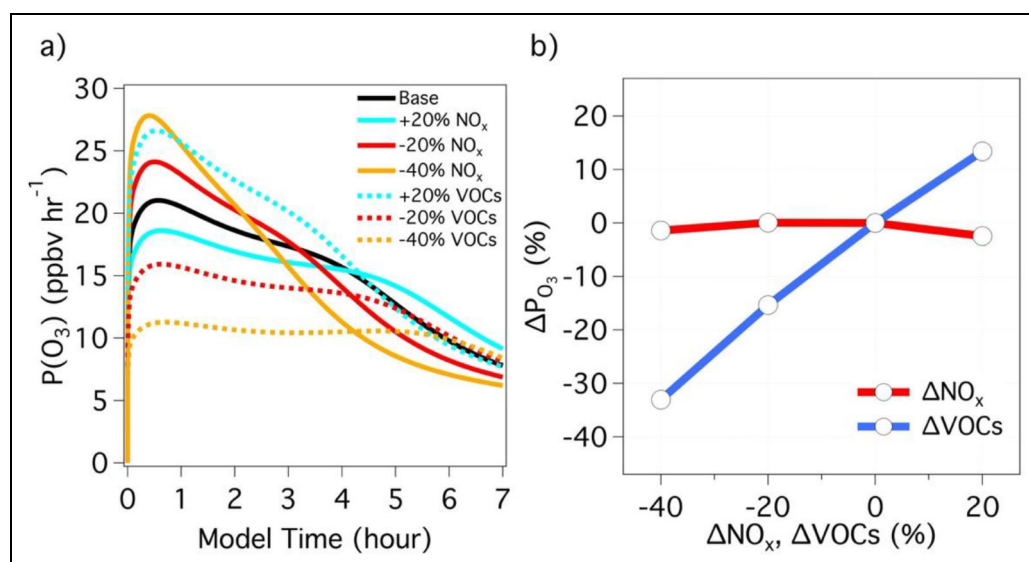Wert et al. (2003) pointed out that observed levels of ethene and propene in the HSC plumes alone explained

Figure 11. The model sensitivity of P(O₃) to perturbations of NOₓ and volatile organic compounds (VOCs) concentrations. (a) The model calculated P(O₃) as a function of model time and (b) the average relative changes of modeled P(O₃), ΔP(O₃), are compared to the base case scenario when model inputs for NOₓ and VOCs were varied by 120%, 80%, and 60% of the base model constraints.

the highest HCHO and ozone levels of over 30 and 200 ppbv, respectively. In the DPCC, high levels of small alkenes significantly impact OH reactivity and ozone production as well. One notable difference between the HSC and the DPCC emissions is the high levels of 1,3-butadiene in the DPCC plumes, where photochemical oxidation of 1,3-butadiene accounted for 17% and 9% of OH reactivity and ozone production, respectively. In contrast, emissions of 1,3-butadiene were a minor contributor to OH reactivity and rapid ozone formation in the HSC (Ryerson et al., 2003). Measurements during the TexAQS and SEAC⁴RS campaigns demonstrated efficient production of HNO_3, PANs, and ANs from oxidations of reactive VOCs with NO_x in petrochemical plumes (Roberts et al., 2003; Ryerson et al., 2003; Rosen et al., 2004; Teng et al., 2015). In particular, elevated levels of short-lived NO_z including HNs and APAN with limited hydrocarbon precursors clearly illustrated the impacts of alkene oxidation on the loss of NO_x (Roberts et al., 2001; Teng et al., 2015). Significant enhancements of HNs and APAN were also observed downwind of major petrochemical facilities including the DPCC and Ulsan petrochemical complex. In our model case study, the production of short-lived NO_z species effectively sequestered NO_x in addition to the loss of NO_x by the formation of HNO_3 and longer lived ANs, which resulted in a NO_x lifetime of 2.6 h over a 7-h model integration. Ryerson et al. (2003) reported a NO_x lifetime in the HSC plumes of 1.8 h, which was markedly shorter than that of power plant plumes (τ_{NO_x} approximately 6 h) (Ryerson et al., 1998).

Although a quantitative comparison of the ozone production between Houston and the DPCC is difficult, the rates of ozone production in the HSC and the DPCC plumes were higher than those in urban plumes (Daum et al., 2003; Ryerson et al., 2003; Wert et al., 2003; Wood et al., 2010). In addition, both the instantaneous

(approximately 6–10) and empirical (approximately 6) OPEs of the DPCC plumes were similar to the empirical OPEs of 6 and 9 for coalesced plumes from urban and petrochemical sources and for isolated petrochemical plumes, respectively, during the TexAQS 2006 campaign (Neuman et al., 2009).

The similarity of previous observations in Houston and this work demonstrates that the emission characteristics and downwind evolution of petrochemical plumes are distinguishable even in heterogeneous VOCs-NO_x environment such as East Asia. This also suggests that reduction in petrochemical VOC emissions, which has been effective in controlling ozone levels in Houston over the past decade, may be effective to reduce downwind ozone production from the DPCC (Kim et al., 2011; Johansson et al., 2014; Zhou et al., 2014). We investigate the validity of this assumption in terms of the sensitivity of P(O₃) to perturbation of NO_x and VOCs in our diagnostic model simulations. **Figure 11a** shows the calculated P(O₃) as a function of model time, when initial constraints for NO_x and VOCs were varied by 120%, 80%, and 60% of the base model constraints used in Section 4.5. **Figure 11b** shows the average relative changes of P(O₃), ΔP(O₃), with respect to those of NO_x and VOCs (ΔNO_x and ΔVOCs). The slightly negative and strongly positive responses of P(O₃) to the perturbation of NO_x and VOCs, respectively, in **Figure 11** illustrate that photochemistry in the DPCC plumes is radical-limited on average, and thus, reduction in VOCs emissions should be a priority for reducing downwind ozone production. Reductions in emissions of small alkenes such as ethene, propene, and 1,3-butadiene are likely an effective mitigation strategy for controlling ozone and potentially SOA production. We suggest that production (petrochemical refining, process, and gas flaring) and fugitive (leaks from pipelines, storage tanks, and valves) emissions are attractive targets as sources of such

alkenes. We emphasize that reduction of 1,3-butadiene emissions is especially important for the local air quality in Daesan area. Although the effects of the DPCC emissions on local and regional air quality in South Korea should be further investigated utilizing in situ measurements and chemical transport modeling, this work points to potentially effective mitigation strategies.

5. Summary and conclusion

Primary petrochemical emissions and secondary photochemical products were measured over the DPCC and the Yellow Sea from the NASA DC-8 research aircraft in 2016. Alkenes such as ethene, propene, butene isomers, and 1,3-butadiene are the dominant contributors to both OH reactivity and ozone production in the DPCC plumes.

The photochemical oxidation of these reactive alkenes resulted in efficient reactive nitrogen processing in the DPCC plumes, where emitted NO_x was converted to HNO_3, PANs, and ANs (>80% of NO_y) within a few hours downwind. The large elevations of the short-lived reactive nitrogen compounds such as HNs and APAN were observed in an intermediate distance from the DPCC and Ulsan Petrochemical Complex and highlighted the photo-oxidation of uniquely speciated petrochemical VOCs emissions with NO_x. The highest ozone levels up to approximately 250 ppbv with elevated levels of APAN and relatively lower contributions of PAN to PANs were observed in the DPCC plumes. Such elevated levels of ozone were consistent with high instantaneous $P(O_3)$ over the DPCC and the Yellow Sea. In addition, estimated instantaneous P(SOA) using updated parameters for SOA yields indicate that the contributions of alkenes to P(SOA) were comparable to more common SOA precursors such as aromatics for petrochemical transects at intermediate distances from the DPCC.

A model case study using a 0-D box model with initial observational constraints, an estimated dilution factor and a near-explicit mechanism was utilized to approximate downwind petrochemical plume chemistry using an example plume similar to the DPCC plume transects. The model reproduced the downwind evolution of ozone and reactive nitrogen compounds such as PANs and HNs to within approximately 40% in general, as well as the rates and efficiency of ozone production based on the observations. The model also simulated enhancements of short-lived reactive nitrogen such as APAN and HNs with specific alkene precursors, where the oxidation of their alkene precursors strongly influences ozone production and reactive nitrogen processing at different stages of downwind plume evolution. The simulated PNs budget indicated the potential for significant levels of rarely measured PAN homologues such as PHAN and PBzN (approximately 20% of the PNs) in petrochemical plumes. Glycolaldehyde and benzaldehyde, secondarily produced from ethene, 1,3-butadiene, and styrene, were major precursors of PHAN and PBzN, respectively, in our model simulations incorporating the MCM. Such rarely measured PAN compounds are potentially present in petrochemical plumes in large levels and are important for understanding the details of ozone production and reactive nitrogen processing.

Finally, many of the observed features of the DPCC plumes were consistent with previous observations in Houston that were impacted by petrochemical emissions. The positive response of ozone production to VOCs in our model analysis points out that reduction of primary VOCs emissions from the DPCC should be a priority for reducing downwind ozone production. Reduction in production and fugitive emissions of light alkenes from petrochemical industrial sources has been effective to control air pollution in Houston over the past decade (Kim et al., 2011; Johansson et al., 2014; Zhou et al., 2014). This work suggests that such emissions, especially of 1,3-butadiene, should be targeted in formulating mitigation strategies for ozone and potentially SOA pollution in the Daesan area.

Competing interests

The authors have no competing interests to declare.

Author contributions

YRL interpreted the data and wrote the manuscript with assistance from LGH. LGH, DJT, and XL collected PANs, SO_2, and HCl data. MT and NLN assisted with the aerosol production calculations. AF and DR provided HCHO measurements. IJS, DRB, NJB, and SM provided the WAS VOC measurements. GSD, JPD, YC, and SEP provided CO, CO_2, and CH_4 measurements. POW, MJK, JDC, and APT provided HNO_3, HNs, dihydroxytoluene, and glycolaldehyde measurements. RCC and PSR provided ANs measurements. WB provided OH and HO_2 measurements. AW and TM provided the PTR-ToF-MS VOC measurements. JLJ, PCJ, and BAN provided the AMS aerosol measurements and assisted in the aerosol production calculations. AW provided NO, NO_2, NO_y, and O_3 measurements. SRH and KU provided photolysis frequencies measurements. All authors contributed to the review and editing of this article.

References

Alvarado, MJ, **Lonsdale, CR**, **Yokelson, RJ**, **Akagi, SK**, **Coe, H**, **Craven, JS**, **Fischer, EV**, **McMeeking, GR**, **Seinfeld, JH**, **Soni, T**, **Taylor, JW**, **Weise, DR**, **Wold, CE**. 2015. Investigating the links between ozone and organic aerosol chemistry in a biomass burning plume from a prescribed fire in California chaparral. *Atmospheric Chemistry and Physics* **15**: 6667–6688. DOI: http://dx.doi.org/10.5194/acp-15-6667-2015.

Atkinson, R, **Arey, J**. 2003. Atmospheric degradation of volatile organic compounds. *Chemical Reviews* **103**: 4605–4638. DOI: http://dx.doi.org/10.1021/cr0206420.

Bahreini, R, **Ervens, B**, **Middlebrook, AM**, **Warneke, C**, **de Gouw, JA**, **DeCarlo, PF**, **Jimenez, JL**, **Brock, CA**, **Neuman, JA**, **Ryerson, TB**, **Stark, H**, **Atlas, EL**, **Brioude, J**, **Fried, A**, **Holloway, JS**, **Peischl, J**, **Ricther, D**, **Walega, J**, **Weibring, P**, **Wollny, AG**, **Fehsenfeld, FC**. 2009. Organic aerosol formation in urban and industrial plumes near Houston and Dallas, Texas. *Journal of Geophysical Research* **114**: D00F16. DOI: http://dx.doi.org/10.1029/2008JD011493.

Bourgeois, I, **Peischl, J**, **Neuman, JA**, **Brown, SS**, **Allen, HM**, **Campuzano-Jost, P**, **Coggon, MM**, **DiGangi, JP**, **Diskin, GS**, **Gilman, JB**, **Gkatzelis, GI**, **Guo, H**, **Halliday, HA**, **Hanisco, TF**, **Holmes, CD**, **Huey, LG**, **Jimenez, JL**, **Lamplugh, AD**, **Lee, YR**, **Lindaas, J**, **Moore, RH**, **Nault, BA**, **Nowak, JB**, **Pagonis, D**, **Rickly, PS**, **Robinson, MA**, **Rollins, AW**, **Selimovic, V**, **St. Clair, JM**, **Tanner, D**, **Vasquez, KT**, **Veres, PR**, **Warneke, C**, **Wennberg, PO**, **Washenfelder, RA**, **Wiggins, EB**, **Womack, CC**, **Xu, L**, **Zarzana, KJ**, **Ryerson, TB**. 2022. Comparison of airborne measurements of NO, NO_2, HONO, NO_y, and CO during FIREX-AQ. *Atmospheric Measurement Techniques* **15**: 4901–4930. DOI: https://dx.doi.org/10.5194/amt-15-4901-2022.

Brock, CA, **Trainer, M**, **Ryerson, TB**, **Neuman, JA**, **Parrish, DD**, **Holloway, JS**, **Nicks, DK Jr**, **Frost, GJ**, **Hubler, G**, **Fehsenfeld, FC**, **Wilson, JC**, **Reeves, JM**, **Lafleur, BG**, **Hilbert, H**, **Atlas, EL**, **Donnelly, SG**, **Schauffler, SM**, **Stroud, VR**, **Wiedinmyer, C**. 2003. Particle growth in urban and industrial plumes in Texas. *Journal of Geophysical Research* **108**: 4111. DOI: http://dx.doi.org/10.1029/2002JD002746.

Chan, AWH, **Chan, MN**, **Surratt, JD**, **Chhabra, PS**, **Loza, CL**, **Crounse, JD**, **Yee, LD**, **Flagan, RC**, **Wennberg, PO**, **Seinfeld, JH**. 2010. Role of aldehyde chemistry and NO_x concentrations in secondary organic aerosol formation. *Atmospheric Chemistry and Physics* **10**: 7169–7188. DOI: http://dx.doi.org/10.5194/acp-10-7169-2010.

Cheng, H, **Sathiakumar, N**, **Graff, J**, **Matthews, R**, **Delzell, E**. 2007. 1,3-Butadiene and leukemia among synthetic rubber industry workers: Exposure–response relationships. *Chemico-Biological Interactions* **166**: 15–24. DOI: http://dx.doi.org/10.1016/j.cbi.2006.10.004.

Cho, C, **St. Clair, JM**, **Liao, J**, **Wolfe, GM**, **Jeong, S**, **Kang, D**, **Choi, J**, **Shin, M-H**, **Park, J**, **Park, J-H**, **Fried, A**, **Weinheimer, A**, **Blake, DR**, **Diskin, GS**, **Ullmann, K**, **Hall, SR**, **Brune, WH**, **Hanisco, TF**, **Min, K-E**. 2021. Evolution of formaldehyde (HCHO) in a plume originating from a petrochemical industry and its volatile organic compounds (VOCs) emission rate estimation. *Elementa: Science of the Anthropocene* **9**: 1. DOI: https://doi.org/10.1525/elementa.2021.00015.

Crawford, JH, **Ahn, J-Y**, **Al-Saadi, J**, **Chang, L**, **Emmons, LK**, **Kim, J**, **Lee, G**, **Park, J-H**, **Park, RJ**, **Woo, JH**, **Song, C-K**, **Hong, J-H**, **Hong, Y-D**, **Lefer, BL**, **Lee, M**, **Lee, T**, **Kim, S**, **Min, K-M**, **Yum, SS**, **Shin, HJ**, **Kim, Y-W**, **Choi, J-S**, **Park, J-S**, **Szykman, JJ**, **Long, RW**, **Jordan, CE**, **Simpson, IJ**, **Fried, A**, **Dibb, JE**, **Cho, SY**, **Kim, YP**. 2021. The Korea–United States Air Quality (KORUS-AQ) field study. *Elementa: Science of the Anthropocene* **9**: 1. DOI: http://dx.doi.org/10.1525/elementa.2020.00163.

Daum, PH, **Kleinman, LI**, **Springston, SR**, **Nunnermacker, LJ**, **Lee, Y-N**, **Weinstein-Lloyd, J**, **Zheng, J**, **Berkowitz, CM**. 2003. A comparative study of O_3 formation in the Houston urban and industrial plumes during the 2000 Texas Air Quality Study. *Journal of Geophysical Research* **108**(D23). DOI: http://dx.doi.org/10.1029/2003JD003552.

Duncan, BN, **Lamsal, LN**, **Thompson, AM**, **Yoshida, Y**, **Lu, Z**, **Streets, DG**, **Hurwitz, MM**, **Pickering, KE**. 2016. A space-based, high-resolution view of notable changes in urban NO_x pollution around the world (2005–2014). *Journal of Geophysical Research* **121**: 976–996. DOI: http://dx.doi.org/10.1002/2015JD024121.

Fried, A, **Walega, J**, **Weibring, P**, **Richter, D**, **Simpson, IJ**, **Blake, DR**, **Blake, NJ**, **Meinardi, S**, **Barletta, B**, **Hughes, SC**, **Crawford, JH**, **Diskin, G**, **Barrick, J**, **Hair, J**, **Fenn, M**, **Wisthaler, A**, **Mikoviny, T**, **Woo, J-H**, **Park, M**, **Kim, J**, **Min, K-E**, **Jeong, S**, **Wennberg, PO**, **Kim, MJ**, **Crounse, JD**, **Teng, AP**, **Bennett, R**, **Yang-Martin, M**, **Shook, MA**, **Huey, G**, **Tanner, D**, **Knote, C**, **Kim, JH**, **Park, R**, **Brune, W**. 2020. Airborne formaldehyde and volatile organic compound measurements over the Daesan petrochemical complex on Korea's northwest coast during the Korea-United States Air Quality study: Estimation of emission fluxes and effects on air quality. *Elementa: Science of the Anthropocene* **8**(1): 121. DOI: http://dx.doi.org/10.1525/elementa.2020.121.

Fung, K, **Grosjean, D**. 1985. Peroxybenzoylnitrate: Measurements in smog chambers and in urban air. *The Science of The Total Environment* **46**: 29–40. DOI: http://dx.doi.org/10.1016/0048-9697(85)90281-5.

Ge, S, **Xu, Y**, **Jia, L**. 2017. Secondary organic aerosol formation from propylene irradiation in a chamber study. *Atmospheric Environment* **157**: 146–155. DOI: http://dx.doi.org/10.1016/j.atmosenv.2017.03.019.

Gilman, JB, **Kuster, WC**, **Goldan, PD**, **Herdon, SC**, **Zahniser, MS**, **Tucker, SC**, **Brewer, WA**, **Lerner, BM**,

Williams, EJ, **Harley, RA**, **Fehsenfeld, FC**, **Warneke, C**, **de Gouw, JA**. 2009. Measurements of volatile organic compounds during the 2006 TexAQS/GoMACCS campaign: Industrial influences, regional characteristics, and diurnal dependencies of the OH reactivity. *Journal of Geophysical Research* **114**: D00F06. DOI: http://dx.doi.org/10.1029/2008JD011525.

Huang, XHH, **Ip, HSS**, **Yu, JZ**. 2011. Secondary organic aerosol formation from ethene in the urban atmosphere of Hong Kong: A multiphase chemical modeling study. *Journal of Geophysical Research* **116**(D03206). DOI: http://dx.doi.org/10.1029/2010JD014121.

International Energy Agency. 2018. The future of petrochemicals. Technology report. Available at https://www.iea.org/reports/the-future-of-petrochemicals.

Jaoui, M, **Lewandowski, M**, **Docherty, K**, **Offenberg, JH**, **Kleindienst, TE**. 2014. Atmospheric oxidation of 1,3-butadiene: Characterization of gas and aerosol reaction products and implication for PM$_{2.5}$. *Atmospheric Chemistry and Physics* **14**: 13681–13704. DOI: http://dx.doi.org/10.5194/acp-14-13681-2014.

Jia, L, **Xu, Y**. 2016. Ozone and secondary organic aerosol formation from ethene-NO$_x$-NaCl irradiations under different relative humidity conditions. *Journal of Atmospheric Chemistry* **73**: 81–100. DOI: http://dx.doi.org/10.1007/s10874-015-9317-1.

Jobson, BT, **Berkowitz, CM**, **Kuster, WC**, **Goldan, PD**, **Williams, EJ**, **Fesenfeld, FC**, **Apel, EC**, **Lonneman, WA**, **Riemer, D**. 2004. Hydrocarbon source signatures in Houston, Texas: Influence of the petrochemical industry. *Journal of Geophysical Research* **109**: D24305. DOI: http://dx.doi.org/10.1029/2004JD004887.

Johansson, JKE, **Mellqvist, J**, **Samuelsson, J**, **Offerle, B**, **Barry, L**, **Rappengluck, B**, **Flynn, J**, **Yarwood, G**. 2014. Emission measurements of alkenes, alkanes, SO$_2$ and NO$_2$ from stationary sources in Southeast Texas over a 5 year period using SOF and mobile DOAS. *Journal of Geophysical Research* **119**: 1973–1991. DOI: http://dx.doi.org/10.1002/2013JD020485.

Jordan, CE, **Crawford, JH**, **Beyersdorf, AJ**, **Eck, TF**, **Halliday, HS**, **Nault, BA**, **Chang, L-S**, **Park, J**, **Park, RJ**, **Lee, G**, **Kim, H**, **Ahn, J-y**, **Cho, S**, **Shin, HJ**, **Lee, JH**, **Jung, JS**, **Kim, D-S**, **Lee, M**, **Lee, T**, **Whitehill, A**, **Szykman, J**, **Schueneman, MK**, **Campuzano-Jost, P**, **Jimenez, JL**, **DiGangi, JP**, **Diskin, GS**, **Anderson, BE**, **Moore, RH**, **Ziemba, LD**, **Fenn, MA**, **Hair, JW**, **Kuehn, RE**, **Holz, RE**, **Chen, G**, **Travis, K**, **Shook, M**, **Peterson, DA**, **Lamb, KD**, **Schwarz, JP**. 2020. Investigation of factors controlling PM$_{2.5}$ variability across the South Korean Peninsula during KORUS-AQ. *Elementa: Science of the Anthropocene* **8**: 28. DOI: http://dx.doi.org/10.1525/elementa.424.

Kim, H, **Gil, J**, **Lee, M**, **Jung, J**, **Whitehill, A**, **Szykman, J**, **Lee, G**, **Kim, D-S**, **Cho, S**, **Ahn, J-Y**, **Hong, J**, **Park, M-S**. 2020. Factors controlling surface ozone in the Seoul Metropolitan Area during the KORUS-AQ campaign. *Elementa: Science of the Anthropocene* **8**: 46. DOI: http://dx.doi.org/10.1525/elementa.444.

Kim, H, **Zhang, Q**, **Heo, J**. 2018. Influence of intense secondary aerosol formation and long-range transport on aerosol chemistry and properties in the Seoul Metropolitan Area during springtime: Results from KORUS-AQ. *Atmospheric Chemistry and Physics* **18**: 7149–7168. DOI: http://dx.doi.org/10.5194/acp-18-7149-2018.

Kim, S, **Sanchez, D**, **Wang, M**, **Seco, R**, **Jeong, D**, **Hughes, S**, **Barletta, B**, **Blake, DR**, **Jung, J**, **Kim, D**, **Lee, G**, **Lee, M**, **Ahn, J**, **Lee, S**, **Cho, G**, **Sung, M**, **Lee, Y**, **Kim, D**, **Kim, Y**, **Woo, J**, **Jo, D**, **Park, R**, **Park, J**, **Hong, Y**, **Hong, J**. 2016. OH reactivity in urban and suburban regions in Seoul, South Korea—An East Asian megacity in a rapid transition. *Faraday Discussion* **189**: 231–251. DOI: http://dx.doi.org/10.1039/c5fd00230c.

Kim, S-W, **McKeen, SA**, **Frost, GJ**, **Lee, S-H**, **Trainer, M**, **Richter, A**, **Angevine, WM**, **Atlas, EL**, **Bianco, L**, **Boersma, KF**, **Brioude, J**, **Burrows, JP**, **de Gouw, JA**, **Fried, A**, **Gleason, J**, **Hillboll, A**, **Mellqvist, J**, **Peischl, J**, **Richter, D**, **Rivera, C**, **Ryerson, TB**, **Hekkert, SL**, **Walega, J**, **Warneke, C**, **Weibring, P**, **Williams, E**. 2011. Evaluations of NO$_x$ and highly reactive VOC emission inventories in Texas and their implications for ozone plume simulations during the Texas Air Quality Study 2006. *Atmospheric Chemistry and Physics* **11**: 11361–11386. DOI: http://dx.doi.org/10.5194/acp-11-11361-2011.

Kim, YP, **Lee, G**. 2018. Trend of air quality in Seoul: Policy and science. *Aerosol and Air Quality Research* **18**: 2141–2156. DOI: http://dx.doi.org/10.4209/aaqr.2018.03.0081.

Kirman, CR, **Albertini, RA**, **Gargas, ML**. 2010. 1,3-Butadiene: III. Assessing carcinogenic modes of action. *Critical Reviews in Toxicology* **40**(sup1): 74–92. DOI: http://dx.doi.org/10.3109/10408444.2010.507183.

Korea Petrochemical Industry Association. 2019. *2019 Petrochemical Industry in Korea*. Seoul, South Korea: Korea Petrochemical Industry Association.

Lee, Y, **Huey, LG**, **Wang, Y**, **Qu, H**, **Zhang, R**, **Ji, Y**, **Tanner, DJ**, **Wang, X**, **Tang, J**, **Song, W**, **Hu, W**, **Zhang, Y**. 2021. Photochemistry of volatile organic compounds in the Yellow River Delta, China: Formation of O$_3$ and peroxyacyl nitrates. *Journal of Geophysical Research* **126**: e2021JD035296. DOI: http://dx.doi.org/10.1029/2021JD035296.

Lindaas, J, **Farmer, DK**, **Pollack, IB**, **Abeleira, A**, **Flocke, F**, **Fischer, EV**. 2019. Acyl peroxy nitrates link oil and natural gas emissions to high ozone abundances in the Colorado Front Range during Summer 2015. *Journal of Geophysical Research* **124**: 2336–2350. DOI: http://dx.doi.org/10.1029/2018JD028825.

Lippmann, M. 1991. Health effects of tropospheric ozone. *Environmental Science & Technology* **25**: 1954–1962. DOI: http://dx.doi.org/10.1021/es00024a001.

Liu, X, Huey, LG, Yokelson, RJ, Selimovic, V, Simpson, IJ, Müller, M, Jimenez, JL, Campuzano-Jost, P, Beyersdorf, AJ, Blake, DR, Butterfield, Z, Choi, Y, Crounse, JD, Day, DA, Diskin, GS, Dubey, MK, Fortner, E, Hanisco, TF, Hu, W, King, LE, Kleinman, L, Meinardi, S, Mikoviny, T, Onasch, TB, Palm, BB, Peischl, J, Pollack, IB, Ryerson, TB, Sachse, GW, Sedlacek, AJ, Shilling, JE, Springston, S, St. Clair, JM, Tanner, DJ, Teng, AP, Wennberg, PO, Wisthaler, A, Wolfe, GM. 2017. Airborne measurements of western U.S. wildfire emissions: Comparison with prescribed burning and air quality implications. *Journal of Geophysical Research* **122**: 6108–6129. DOI: http://dx.doi.org/10.1002/2016JD026315.

Liu, X, Zhang, Y, Huey, LG, Yokelson, RJ, Wang, Y, Jimenez, JL, Campuzano-Jost, P, Beyersdorf, AJ, Blake, DR, Choi, Y, St. Clair, JM, Crounse, JD, Day, DA, Diskin, GS, Fried, A, Hall, SR, Hanisco, TF, King, LE, Meinardi, S, Mikoviny, T, Palm, BB, Peischl, J, Perring, AE, Pollack, IB, Ryerson, TB, Sachse, G, Schwarz, JP, Simpson, IJ, Tanner, DJ, Thornhill, KL, Ullmann, K, Weber, RJ, Wennberg, PO, Wisthaler, A, Wolfe, GM, Ziemba, LD. 2016. Agricultural fires in the southeastern U.S. during SEAC⁴RS: Emissions of trace gases and particles and evolution of ozone, reactive nitrogen, and organic aerosol. *Journal of Geophysical Research: Atmospheres* **121**: 7383–7414.

Ma, PK, Zhao, Y, Robinson, AL, Worton, DR, Goldstein, AH, Ortega, AM, Jimenez, JL, Zotter, P, Prevot, ASH, Szidat, S, Hayes, PL. 2017. Evaluating the impact of new observational constraints on P-S/IVOC emissions, multi-generation oxidation, and chamber wall losses on SOA modeling for Los Angeles, CA. *Atmospheric Chemistry and Physics* **17**: 9237–9259. DOI: http://dx.doi.org/10.5194/acp-17-9237-2017.

Meijer, GM, Neiboer, H. 1978. Determination of peroxybenzoyl nitrate (PBzN) in ambient air, in Guicherit, R ed., *Photochemical smog formation in the Netherlands.* Delft, Netherlands: TNO's-Gravenhage: 60–63.

Nault, BA, Campuzano-Jost, P, Day, DA, Schroder, JC, Anderson, B, Beyersdorf, AJ, Blake, DR, Brune, WH, Choi, Y, Corr, CA, de Gouw, JA, Dibb, J, DiGangi, JP, Diskin, GS, Fried, A, Huey, LG, Kim, MJ, Knote, CJ, Lamb, KD, Lee, T, Park, T, Pusede, SE, Scheuer, E, Thornhill, KL, Woo, J-H, Jimenez, JL. 2018. Secondary organic aerosol production from local emissions dominates the organic aerosol budget over Seoul, South Korea, during KORUS-AQ. *Atmospheric Chemistry and Physics* **18**: 17769–17800. DOI: http://dx.doi.org/10.5194/acp-18-17769-2018.

Nault, BA, Jo, DS, McDonald, BC, Campuzano-Jost, P, Day, DA, Hu, W, Schroder, JC, Allan, J, Blake, DR, Canagaratna, MR, Coe, H, Coggon, MM, DeCarlo, PF, Diskin, GS, Dunmore, R, Flocke, F, Fried, A, Gilman, JB, Gkatzelis, G, Hamilton, JF, Hanisco, TF, Hayes, PL, Henze, DK, Hodzic, A, Hopkins, J, Hu, M, Huey, LG, Jobson, BT, Kuster, WC, Lewis, A, Li, M, Liao, J, Nawaz, MO, Pollack, IB, Peischl, J, Rappenglück, B, Reeves, CE, Richter, D, Roberts, JM, Ryerson, TB, Shao, M, Sommers, JM, Walega, J, Warneke, C, Weibring, P, Wolfe, GM, Young, DE, Yuan, B, Zhang, Q, de Gouw, JA, Jimenez, JL. 2021. Secondary organic aerosols from anthropogenic volatile organic compounds contribute substantially to air pollution mortality. *Atmospheric Chemistry and Physics* **21**: 11201–11224. DOI: http://dx.doi.org/10.5194/acp-21-11201-2021.

Neuman, JA, Aikin, KC, Atlas, EL, Blake, DR, Holloway, JS, Meinardi, S, Nowak, JB, Parrish, DD, Peischl, J, Perring, AE, Pollack, IB, Roberts, JM, Ryerson, TB, Trainer M. 2012. Ozone and alkyl nitrate formation from the Deepwater Horizon oil spill atmospheric emissions. *Journal of Geophysical Research* **117**: D09305. DOI: http://dx.doi.org/10.1029/2011JD017150.

Neuman, JA, Nowak, JB, Zheng, W, Flocke, F, Ryerson, TB, Trainer, M, Holloway, JS, Parrish, DD, Frost, GJ, Peischl, J, Atlas, EL, Bahreini, R, Wollny, AG, Fehsenfeld, FC. 2009. Relationship between photochemical ozone production and NO_x oxidation in Houston, Texas. *Journal of Geophysical Research* **114**: D00F08. DOI: http://dx.doi.org/10.1029/2008JD011688.

Niki, H, Maker, PD, Savage, CM, Hurley, MD. 1987. Fourier transform infrared study of the kinetics and mechanisms for the Cl-atom- and HO-radical-initiated oxidation of glycolaldehyde. *Journal of Physical Chemistry* **91**: 2174–2178. DOI: http://dx.doi.org/10.1021/j100292a038.

Oak, YJ, Park, RJ, Schroeder, JR, Crawford, JH, Blake, DR, Weinheimer, AJ, Woo, J-H, Kim, S-W, Yeo, H, Fried, A, Wisthaler, A, Brune, WH. 2019. Evaluation of simulated O_3 production efficiency during the KORUS-AQ campaign: Implications for anthropogenic NO_x emissions in Korea. *Elementa: Science of the Anthropocene* **7**: 56. DOI: http://dx.doi.org/10.1525/elementa.394.

Orlando, JJ, Tyndall, GS. 2002. Mechanisms for the reactions of OH with two unsaturated aldehydes: Crotonaldehyde and acrolein. *Journal of Physical Chemistry* **106**: 12252–12259. DOI: http://dx.doi.org/10.1021/jp021530f.

Perring, AE, Bertram, TH, Farmer, DK, Wooldridge, PJ, Dibb, J, Blake, NJ, Blake, DR, Singh, HB, Fuelberg, H, Diskin, G, Sachse, G, Cohen, RC. 2010. The production and persistence of $\Sigma RONO_2$ in the Mexico City plume. *Atmospheric Chemistry and Physics* **10**: 7215–7229. DOI: http://dx.doi.org/10.5194/acp-10-7215-2010.

Perring, AE, Pusede, SE, Cohen, RC. 2013. An observational perspective on the atmospheric impacts of alkyl and multifunctional nitrates on ozone and secondary organic aerosol. *Chemical Reviews* **113**: 5848–5870. DOI: http://dx.doi.org/10.1021/cr300520x.

Peterson, DA, **Hyer, EJ**, **Han, S-O**, **Crawford, JH**, **Park, RJ**, **Holz, R**, **Kuehn, RE**, **Eloranta, E**, **Knote, C**, **Jordan, CE**, **Lefer, BL**. 2019. Meteorology influencing springtime air quality, pollution transport, and visibility in Korea. *Elementa: Science of the Anthropocene* **7**(1): 57. DOI: http://dx.doi.org/10.1525/elementa.395.

Roberts, JM. 2007. *PAN and related compounds. Volatile organic compounds in the atmosphere.* New York, NY: Wiley Online Library: 221–268.

Roberts, JM, **Flocke, F**, **Weinheimer, A**, **Tanimoto, H**, **Jobson, BT**, **Riemer, D**, **Apel, EC**, **Atlas, EL**, **Donnelly, S**, **Stroud, V**, **Johnson, K**, **Weaver, R**, **Fehsenfeld, FC**. 2001. Observations of APAN during TexAQS 2000. *Geophysical Research Letters* **28**: 4195–4198. DOI: http://dx.doi.org/10.1029/2001GL013466.

Roberts, JM, **Jobson, BT**, **Kuster, W**, **Goldan, P**, **Murphy, P**, **Williams, E**, **Frost, G**, **Riemer, D**, **Apel, E**, **Stroud, C**, **Wiedinmyer, C**, **Fehsenfeld, F**. 2003. An examination of the chemistry of peroxycarboxylic nitric anhydrides and related volatile organic compounds during Texas Air Quality Study 2000 using ground-based measurements. *Journal of Geophysical Research* **108**(D16). DOI: http://dx.doi.org/10.1029/2003JD003383.

Rosen, RS, **Wood, EC**, **Wooldridge, PJ**, **Thornton, JA**, **Day, DA**, **Kuster, W**, **Williams, EJ**, **Cohen, RC**. 2004. Observations of total alkyl nitrates during Texas Air Quality Study 2000: Implications for O_3 and alkyl nitrate photochemistry. *Journal of Geophysical Research* **109**: D07303. DOI: http://dx.doi.org/10.1029/2003JD004227.

Ryerson, TB, **Buhr, MP**, **Frost, GJ**, **Goldan, PD**, **Holloway, JS**, **Hubler, G**, **Jobson, BT**, **Kuster, WC**, **McKeen, SA**, **Parrish, DD**, **Roberts, JM**, **Sueper, DT**, **Trainer, M**, **Williams, J**, **Fehsenfeld, FC**. 1998. Emissions lifetimes and ozone formation in power plant plumes. *Journal of Geophysical Research* **103**: 22569–22583. DOI: http://dx.doi.org/10.1029/98JD01620.

Ryerson, TB, **Trainer, M**, **Angevine, WM**, **Brock, CA**, **Dissly, RW**, **Fehsenfeld, FC**, **Frost, GJ**, **Goldan, PD**, **Holloway, JS**, **Hübler, G**, **Jakoubek, RO**, **Kuster, WC**, **Neuman, JA**, **Nicks, DK Jr**, **Parrish, DD**, **Roberts, JM**, **Sueper, DT**, **Atlas, EL**, **Donnelly, SG**, **Flocke, F**, **Fried, A**, **Potter, WT**, **Schauffler, S**, **Stroud, V**, **Weinheimer, AJ**, **Wert, BP**, **Wiedinmyer, C**, **Alvarez, RJ**, **Banta, RM**, **Darby, LS**, **Senff, CJ**. 2003. Effect of petrochemical industrial emissions of reactive alkenes and NO_x on tropospheric ozone formation in Houston, Texas. *Journal of Geophysical Research* **108**(D8): 4249. DOI: https://doi.org/10.1029/2002JD003070.

Sato, K, **Nakao, S**, **Clark, CH**, **Qi, L**, **Cocker, DR III**. 2011. Secondary organic aerosol formation from the photooxidation of isoprene, 1,3-butadiene, and 2,3-dimethyl-1,3-butadiene under high NO_x conditions. *Atmospheric Chemistry and Physics* **11**: 7301–7317. DOI: http://dx.doi.org/10.5194/acp-11-7301-2011.

Schroeder, JR, **Crawford, JH**, **Ahn, J-Y**, **Chang, L**, **Fried, A**, **Walega, J**, **Weinheimer, A**, **Montzka, DD**, **Hall, SR**, **Ullmann, K**, **Wisthaler, A**, **Mikoviny, T**, **Chen, G**, **Blake, DR**, **Blake, NJ**, **Hughes, SC**, **Meinardi, S**, **Diskin, G**, **Digangi, JP**, **Choi, Y**, **Pusede, SE**, **Huey, GL**, **Tanner, DJ**, **Kim, M**, **Wennberg, PO**. 2020. Observation-based modeling of ozone chemistry in the Seoul metropolitan area during the Korea-United States Air Quality Study (KORUS-AQ). *Elementa: Science of the Anthropocene* **8**(1): 3. DOI: http://dx.doi.org/10.1525/elementa.400.

Simpson, IJ, **Blake, DR**, **Blake, NJ**, **Meinardi, S**, **Barletta, B**, **Hughes, SC**, **Fleming, LT**, **Crawford, JH**, **Diskin, GS**, **Emmons, LK**, **Fried, A**, **Guo, H**, **Peterson, DA**, **Wisthaler, A**, **Woo, J-H**, **Barré, J**, **Gaubert, B**, **Kim, J**, **Kim, MJ**, **Kim, Y**, **Knote, C**, **Mikoviny, T**, **Pusede, SE**, **Schroeder, JR**, **Wang, Y**, **Wennberg, PO**, **Zeng, L**. 2020. Characterization, sources and reactivity of volatile organic compounds (VOCs) in Seoul and surrounding regions during KORUS-AQ. *Elementa: Science of the Anthropocene* **8**(1): 37. DOI: http://dx.doi.org/10.1525/elementa.434.

Simpson, IJ, **Marrero, JE**, **Batterman, S**, **Meinardi, S**, **Barletta, B**, **Blake, DR**. 2013. Air quality in the industrial Heartland of Alberta, Canada and potential impacts on human health. *Atmospheric Environment* **81**: 702–709. DOI: http://dx.doi.org/10.1016/j.atmosenv.2013.09.017.

Snyder, R. 2002. Benzene and leukemia. *Critical Reviews in Toxicology* **32**(3): 155–210. DOI: http://dx.doi.org/10.1080/20024091064219.

Sprengnether, M, **Demerjian, KL**, **Donahue, NM**, **Anderson, JG**. 2002. Product analysis of the OH oxidation of isoprene and 1,3-butadiene in the presence of NO. *Journal of Geophysical Research* **107**(D15). DOI: http://dx.doi.org/10.1029/2001JD000716.

Stein, AF, **Draxler, RR**, **Rolph, GD**, **Stunder, BJB**, **Cohen, MD**, **Ngan, F**. 2015. NOAA's HYSPLIT atmospheric transport and dispersion modeling system. *Bulletin of the American Meteorological Society* **96**(12): 2059–2077. DOI: http://dx.doi.org/10.1175/bams-d-14-00110.1.

Teng, AP, **Crounse, JD**, **Lee, L**, **St. Clair, JM**, **Cohen, RC**, **Wennberg, PO**. 2015. Hydroxy nitrate production in the OH-initiated oxidation of alkenes. *Atmospheric Chemistry and Physics* **15**: 4297–4316. DOI: http://dx.doi.org/10.5194/acp-15-4297-2015.

Toon, OB, **Maring, H**, **Dibb, J**, **Ferrare, R**, **Jacob, DJ**, **Jensen, EJ**, **Luo, ZJ**, **Mace, GG**, **Pan, LL**, **Pfister, L**, **Rosenlof, KH**, **Redemann, J**, **Reid, JS**, **Singh, HB**, **Thompson, AM**, **Yokelson, R**, **Minnis, P**, **Chen, G**, **Jucks, KW**, **Pszenny, A**. 2016. Planning, implementation, and scientific goals of the Studies of Emissions and Atmospheric Composition, Clouds and Climate Coupling by Regional Surveys (SEAC[4]RS) field mission. *Journal of Geophysical Research* **121**: 4967–5009. DOI: http://dx.doi.org/10.1002/2015JD024297.

Travis, KR, **Crawford, JH**, **Chen, G**, **Jordan, CE**, **Nault, BA**, **Kim, H**, **Jimenez, JL**, **Campuzano-Jost, P**, **Dibb, JE**, **Woo, JH**, **Kim, Y**, **Zhai, S**, **Wang, X**, **McDuffie, EE**, **Luo, G**, **Yu, F**, **Kim, S**, **Simpson, IJ**, **Blake, DR**, **Chang, L**, **Kim, MJ**. 2022. Limitations in representation of physical processes prevent successful simulation of $PM_{2.5}$ during KORUS-AQ. *Atmospheric Chemistry and Physics Discussion*, in review. DOI: http://dx.doi.org/10.5194/acp-2021-946.

Treves, K, **Rudich, Y**. 2003. The atmospheric fate of C_3–C_6 hydroxyalkyl nitrates. *Journal of Physical Chemistry* **107**: 7809–7817. DOI: http://dx.doi.org/10.1021/jp035064l.

Volkamer, R, **Ziemann, PJ**, **Molina, MJ**. 2009. Secondary organic aerosol formation from acetylene (C_2H_2): Seed effect on SOA yields due to organic photochemistry in the aerosol aqueous phase. *Atmospheric Chemistry and Physics* **9**: 1907–1928. DOI: http://dx.doi.org/10.5194/acp-9-1907-2009.

Washenfelder, RA, **Trainer, M**, **Frost, GJ**, **Ryerson, TB**, **Atlas, EL**, **de Gouw, JA**, **Flocke, FM**, **Fried, A**, **Holloway, JS**, **Parrish, DD**, **Peischl, J**, **Richter, D**, **Schauffler, SM**, **Walega, JG**, **Warneke, C**, **Weibring, P**, **Zheng, W**. 2010. Characterization of NO_x, SO_2, ethene, and propene from industrial emission sources in Houston, Texas. *Journal of Geophysical Research* **115**: D16311. DOI: http://dx.doi.org/10.1029/2009JD013645.

Wert, BP, **Trainer, M**, **Fried, A**, **Ryerson, TB**, **Henry, B**, **Potter, W**, **Angevine, WM**, **Atlas, EL**, **Donnelly, SG**, **Fehsenfeld, FC**, **Frost, GJ**, **Goldan, PD**, **Hansel, A**, **Holloway, JS**, **Hubler, G**, **Kuster, WC**, **Nicks, DK Jr**, **Neuman, JA**, **Parrish, DD**, **Schauffler, S**, **Stutz, J**, **Sueper, DT**, **Wiedinmyer, C**, **Wisthaler, A**. 2003. Signatures of terminal alkene oxidation in airborne formaldehyde measurements during TexAQS 2000. *Journal of Geophysical Research* **108**: 4104. DOI: http://dx.doi.org/10.1029/2002JD002502.

Wolfe, GM, **Cantrell, C**, **Kim, S**, **Mauldin, RL III**, **Karl, T**, **Harley, P**, **Turnispeed, A**, **Zheng, W**, **Flocke, F**, **Apel, EC**, **Hornbrook, RS**, **Hall, SR**, **Ullmann, K**, **Henry, SB**, **DiGangi, JP**, **Boyle, ES**, **Kaser, L**, **Schnitzhofer, R**, **Hansel, A**, **Graus, M**, **Nakashima, Y**, **Kajii, Y**, **Geunther, A**, **Keutsch, FN**. 2014. Missing peroxy radical sources within a summertime ponderosa pine forest. *Atmospheric Chemistry and Physics* **14**: 4715–4732. DOI: http://dx.doi.org/10.5194/acp-14-4715-2014.

Wolfe, GM, **Hanisco, TF**, **Arkinson, HL**, **Blake, DR**, **Wisthaler, A**, **Mikoviny, T**, **Ryerson, TB**, **Pollack, I**, **Peischl, J**, **Wennberg, PO**, **Crounse, JD**, **St. Clair, JM**, **Teng, A**, **Huey, LG**, **Liu, X**, **Fried, A**, **Weibring, P**, **Richter, D**, **Walega, J**, **Hall, SR**, **Ullmann, K**, **Jimenez, JL**, **Campuzano-Jost, P**, **Bui, TP**, **Diskin, G**, **Podolske, JR**, **Sachse, G**, **Cohen, RC**. 2022. Photochemical evolution of the 2013 California Rim Fire: Synergistic impacts of reactive hydrocarbons and enhanced oxidants. *Atmospheric Chemistry and Physics* **22**: 4253–4275. DOI: http://dx.doi.org/10.5194/acp-22-4253-2022.

Wolfe, GM, **Marvin, MR**, **Roberts, SJ**, **Travis, KR**, **Liao, J**. 2016. The Framework for 0-D Atmospheric Modeling (F0AM) v3.1. *Geoscientific Model Development* **9**: 3309–3319. DOI: http://dx.doi.org/10.5194/gmd-9-3309-2016.

Wood, EC, **Canagaratna, MR**, **Herndon, SC**, **Onasch, TB**, **Kolb, CE**, **Worsnop, DR**, **Kroll, JH**, **Knighton, WB**, **Seila, R**, **Zavala, M**, **Molina, LT**, **DeCarlo, PF**, **Jimenez, JL**, **Weinheimer, AJ**, **Knapp, DJ**, **Jobson, BT**, **Stutz, J**, **Kuster, WC**, **Williams, EJ**. 2010. Investigation of the correlation between odd oxygen and secondary organic aerosol in Mexico City and Houston. *Atmospheric Chemistry and Physics* **10**: 8947–8968. DOI: http://dx.doi.org/10.5194/acp-10-8947-2010.

Wooldridge, PJ, **Perring, AE**, **Bertram, TH**, **Flocke, FM**, **Roberts, JM**, **Singh, HB**, **Huey, LG**, **Thorton, JA**, **Wolfe, GM**, **Murphy, JG**, **Fry, JL**, **Rollins, AW**, **LaFranchi, BW**, **Cohen, RC**. 2010. Total peroxy nitrates (PNs) in the atmosphere: The thermal dissociation-laser induced fluorescence (TD-LIF) technique and comparisons to speciated PAN measurements. *Atmospheric Measurement Technique* **3**: 593–607. DOI: http://dx.doi.org/10.5194/amt-3-593-2010.

Yuan, B, **Wu, WW**, **Shao, M**, **Wang, M**, **Chen, WT**, **Lu, SH**, **Zheng, LM**, **Hu, M**. 2013. VOC emissions, evolutions and contributions to SOA formation at a receptor site in eastern China. *Atmospheric Chemistry and Physics* **13**: 8815–8832. DOI: http://dx.doi.org/10.5194/acp-13-8815-2013.

Zheng, W, **Flocke, F**, **Roberts, JM**, **Ryerson, TB**, **Atlas, E**. 2007. Aircraft measurement of PANs during TexAQS 2006. TexAQS II Principal Finding Data Analysis Workshop. Available at https://csl.noaa.gov/projects/2006. Accessed December 14, 2022.

Zheng, W, **Flocke, FM**, **Tyndall, GS**, **Swanson, A**, **Orlando, JJ**, **Roberts, JM**, **Huey, LG**, **Tanner, DJ**. 2011. Characterization of a thermal decomposition chemical ionization mass spectrometer for the measurement of peroxy acyl nitrates (PANs) in the atmosphere. *Atmospheric Chemistry and Physics* **11**: 6529–6547. DOI: http://dx.doi.org/10.5194/acp-11-6529-2011.

Zhou, W, **Cohan, DS**, **Henderson, BH**. 2014. Slower ozone production in Houston, Texas following emission reductions: Evidence from Texas Air Quality Studies in 2000 and 2006. *Atmospheric Chemistry and Physics* **14**: 2777–2788. DOI: http://dx.doi.org/10.5194/acp-14-2777-2014.

Elem Sci Anth is a peer-reviewed open access journal published by University of California Press.

OPEN ACCESS